

MICROCOPY RESOLUTION TEST CHART
NATIONAL BUREAU OF STANDARDS 1963-A

AD A I 0 8 I 3 2

INVESTIGATION OF A 460 nm XeF LASER
FINAL REPORT

CONTRACT #ONR: N00014-78-C-0343
ARPA #NR-395-568/12-6-77 (421)

Affected Date
October 1, 1977
Completion Date
May 31, 1980

C.H. Fisher, Principal Investigator
(206) 827-0460

To
Office of Naval Research
800 N. Quincy St.
Arlington, VA 22217

By
MATHEMATICAL SCIENCES NORTHWEST, INC.
2755 Northup Way
Bellevue, WA 98004

RECEIVED
OCT 18 1981
A

has been approved
and sale its

The views and conclusions contained in this document are those of the authors and should not be interpreted as necessarily representing the official policies, either expressed or implied, of the Defense Advanced Research Projects Agency or the U.S. Government.

LIST OF FIGURES

<u>Figure</u>		<u>Page</u>
2-1	Schematic Diagram of the XeF 460 nm Laser Induced Fluorescence Experiment	2-6
2-2	Oscilloscope Traces Showing the Exciting Laser Pulse and the Subsequent 460 nm Fluorescence	2-11
3-1	Oscilloscope Traces Showing the Temporal History	3-19
3-2	Time Correlated Oscillograms	3-24
3-3	Densitometer Tracings of Plates Taken	3-26
4-1	Schematic Diagram of the Multipass Amplifier Experiment.	4-30
4-2	Oscilloscope Traces Showing Temporal Dependence	4-33
4-3	Spectra of the Stimulated Emission	4-35
4-4	Laser Energy As a Function of Wavelength for XeF C A Multipass Amplifier	4-37
5-1	Electron Gun Current and Voltage Waveforms	5-41
5-2		
5-3	0.5 m Cooled XeF Laser Chamber	5-46
5-4	Diagram of Apparatus Used for XeF Gain	5-48

<u>Figure</u>		<u>Page</u>
	Measurements	
5-5	Experimental Setup for XeF (C A) Pulsed Gain/Absorption Measurements	5-50
5-6	Room Temperature Gain/Absorption Data Obtained Using the cw Ar ⁺ Laser Probe	5-53
5-7	Room Temperature Gain Data Obtained at 488.0 nm With the Pulsed Dye Laser Probe	5-55
5-8	Time Resolved Profiles	5-58
5-9	Time Resolved Profiles	5-60
5-10	Time Resolved Profiles	5-61
5-11	Time Resolved Profiles	5-63
5-12	Time Integrated Spectra	5-64
5-13	XeF Formation Pathways: Ne Diluent	5-67
5-14	XeF Formation Pathways: Ar Diluent	5-68
5-15	XeF Formation Pathways: Kr Diluent	5-69
5-16	Code Predictions for Ne/Xe/NF ₃ Mixtures	5-73
5-17	XeF* (B X) Power Extraction for Ne/Xe/NF ₃ Mixtures	5-74
5-18	Code Predictions for Ar/Xe/NF ₃ Mixtures	5-75

<u>Figure</u>		<u>Page</u>
5-19	Code Predictions for XeF Performance Kr Diluent	5-76
5-20	Code Predictions for XeF Performance	5-77

I. INTRODUCTION

The rare gas halide lasers have been extensively developed into efficient, high energy lasers operating in the near ultraviolet region of the spectrum. Until recently, most of the development in XeF had concentrated on the B→X transition at 350 nm. There is an even longer wavelength transition in XeF, the C-A continuum band at 460 nm. This transition has had several advantages over the shorter wavelength transitions in existing XeF and KrF lasers, including tunability and optimum atmospheric and aquatic transmission. The purpose of this program was to demonstrate lasing on the C-A transition of XeF and to gather the kinetic data necessary to optimize the laser performance.

The 460 nm kinetics program was designed to measure the radiative lifetime and collisional quenching rate constants for the C state of XeF. These measurements used a state selective, laser induced fluorescence technique developed by MSNW previously to study the XeF(B) state kinetics.¹ These measurements and their interpretation are discussed in Section II.

Experiments to probe for gain using an argon ion laser were conducted at MSNW in He/Xe/NF₃ mixtures excited by a uv preionized electric discharge. These experiments demonstrated that small signal gains of the order of 0.5 to 1.0 percent cm⁻¹ could be achieved at several wavelengths in the 460 nm band. Stimulated emission was obtained from this fast discharge by installing a high Q cavity on the laser

cell. Although the energy obtained when the uv preionized discharge was operated as an oscillator with internal mirrors was only about 50 μJ , this was increased to 4 mJ by injecting a dye laser into a multipass amplifier configuration. The output of the amplifier was tuned from 460 to 510 nm by tuning the injected dye laser pulse. These experiments are described in the two journal articles included in Section III.

The relatively poor performance obtained with the uv preionized discharge devices results from the low value of the small signal gain coupled with the short time available for the buildup of stimulated emission. The most obvious way around this difficulty is to extend the pumping pulse duration. This can be achieved by using e-beam excitation, which can have pulse durations of approximately 1 μsec instead of the 30 nsec possible with the uv preionized discharge. Although the pump power density is lower, resulting in a lower value for the small signal gain, the energy deposition is considerably higher, which should yield a much larger value for the gain-time product.

The feasibility of making an e-beam excited XeF C \rightarrow A laser was investigated by measuring the gain at 488 nm as a function of gas composition, pressure and temperature. Once the optimum conditions had been determined, lasing was demonstrated using a high Q, optical cavity. The laser performance was significantly improved when Kr was used as the diluent. However, even with Kr diluent, the laser did not reach saturation by the end of the 0.9 μsec e-beam pulse.

A computer model, developed at MSNW for the e-beam excited XeF B \rightarrow X laser, was modified to include the known information on the formation and loss of the C state and on the absorption in the 460 nm band. The code predicted

higher net gains than were observed experimentally, suggesting that the absorption was probably higher than predicted. The results of the e-beam excited experiments and the comparison of the model predictions with experiment are presented in Section IV.

REFERENCES

1. C.H. Fisher and R.E. Center, J. Chem. Phys. 69, 2011 (1978).
2. J.M. Harris, F.E. Lytle, and T.C. McCain, Anal. Chem. 48, 2095 (1976).

II. XeF C STATE KINETICS

We have used a state selective laser induced fluorescence technique to investigate the collisional quenching of the XeF 460 nm broadband emission. This optical technique yields quenching rate coefficients which are easier to interpret because there is no interference from charged particles or other excited states.

The experimental technique is similar to that used previously by us to study the quenching of XeF(B) state.¹ A schematic diagram of the experimental apparatus is shown in Figure 2-1. F atoms are produced by flash dissociating a mixture of UF₆ and Xe diluted in another rare gas (He or Ne). After a delay of a few tenths of a millisecond the ground state XeF molecules formed by recombination are excited to the B state with a 351 nm laser pulse. The subsequent fluorescence decay is monitored with a fast photomultiplier and transient digitizer.

The fluorescence cell was constructed of quartz and had uv grade quartz windows fused to it in a cross configuration. Scattered light was a serious problem because a baffle structure to reduce scattered light could not be put into the cell due to the corrosive gases used in the experiments. The fluorescence cell was placed inside a double ellipsoidal reflector with the cell along the common axis and a flashlamp on each of the other axis to obtain maximum coupling of the flashlamp light into the cell. The flashlamps (ILC 4D3) are dye laser lamps designed for short pulse operation and to quench more rapidly than standard

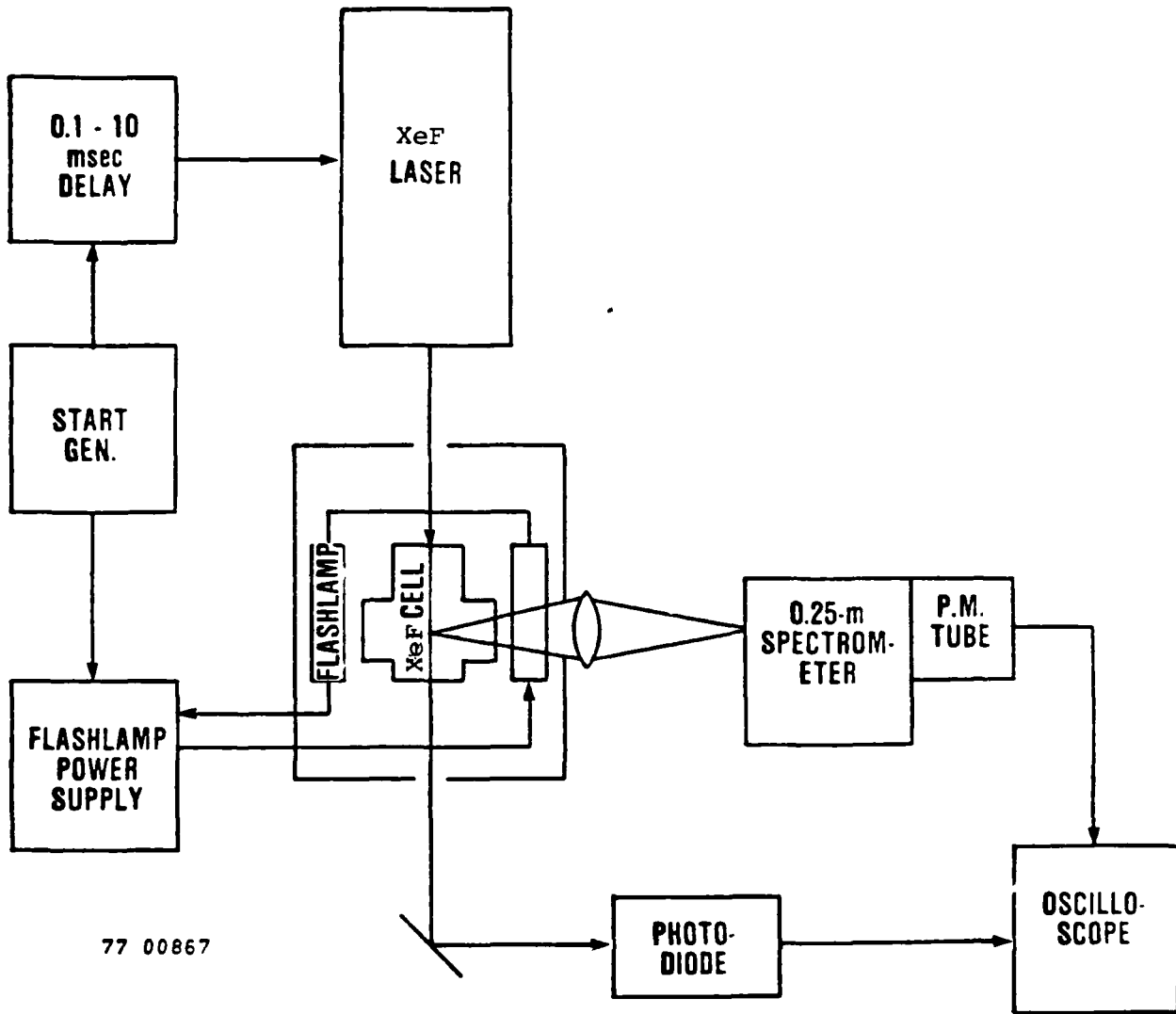


Figure 2-1. Schematic Diagram of the XeF 460 nm Laser Induced Fluorescence Experiment.

flashlamps. The lamps were connected in series and driven from a capacitor which stored 100 J at 10 kV.

The fluorescence cell and its gas manifold were pumped by an oil diffusion pump equipped with an anti-creep, liquid nitrogen cooled baffle. The cell and the stainless steel manifold were well passivated before being used. The quenching gas mixtures were premixed in stainless steel cylinders and allowed to stand overnight to assure good mixing. Gas pressures up to 1000 torr were measured with a capacitance manometer (MKS Baratron 310 BHS-1000) and higher pressures were measured with Bourdon gauges. These mixtures were made up with the correct concentration ratios at ten times the final pressure to reduce errors in measuring the low pressure constituents.

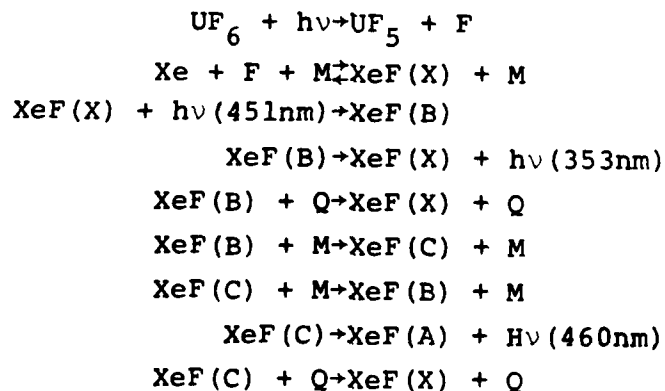
The XeF laser was a discharge laser with ultraviolet spark preionization and excited by a Blumlein transmission line. The laser produced approximately 10 mJ at 25 kV but was normally operated at less than the optimum pressure (2 atm) to obtain a shorter pulse duration (10 nsec FWHM) with a fast decay. The laser was refocussed into the cell by a two lens combination having a long equivalent focal length. The spot size at the viewing plane of the photomultiplier tube was 2 x 4 mm. The lineup of the laser with respect to the fluorescence cell was critical in order to minimize scattered light.

The fluorescence was viewed normal to the exciting laser beam and was reimaged onto the photomultiplier with a 25 mm focal length lens. Broadband emission at 460 nm originating from the XeF(C-A) transition was isolated with a 100 nm bandwidth interference filter centered at 498 nm

combined with a long wave pass color filter to help block the 351 nm exciting light. The exciting laser pulse was isolated with a 350 nm interference filter and monitored with a vacuum photodiode (ITT F4000-S5) which has a time response of less than 1 nsec. The fluorescence was detected with a modified RCA 1P28 photomultiplier tube. The tube base was removed and replaced with a piece of circuit board soldered directly to the tube leads to give faster time response.² By comparing the 351 nm scattered light signal detected with the photomultiplier to the photodiode signal, it was shown that the laser pulse duration and decay time determined the minimum time response of the system (~5 nsec). The quenching data obtained during these experiments were displayed on a 400 MHz oscilloscope (Tektronix 7844) and photographed on Polaroid film. The traces were then digitized from the Polaroid photographs for computer analysis.

Data Analysis

The sequence of reactions describing the formation and decay of XeF^* in our laser induced fluorescence experiment is as follows:



These reactions can be combined to give the following differential equations describing the formation and decay of the XeF B and C states:

$$\frac{dB}{dt} = -\Gamma_B B + \Gamma_{CB} C + P(t)$$

$$\frac{dC}{dt} = -\Gamma_C C + \Gamma_{BC} B$$

where

$$\Gamma_B = \frac{1}{\tau_B} + \Sigma k_Q^B Q + \Sigma k_{BC} M$$

$$\Gamma_C = \frac{1}{\tau_C} + \Sigma k_Q^C Q + \Sigma k_{CB} M$$

$$\Gamma_{BC} = \Sigma k_{BC} M$$

$$\Gamma_{CB} = \Sigma k_{CB} M = \Gamma_{BC} / K_{eq}$$

Here $P(t) = I_{351}(t) [XeF(X)]$ is the pumping term, Γ_B and Γ_C are the loss rates for the B and C states due to radiation and collisional quenching, and Γ_{BC} and Γ_{CB} are the B and C states collisional transfer rates. The solution to these coupled equations is

$$B(t) = \int_0^t P(\lambda) F(t-\lambda) d\lambda$$

$$C(t) = \int_0^t P(\lambda) G(t-\lambda) d\lambda$$

$$\text{with } F(t) = (\gamma_f - \gamma_s)^{-1} \left[(\Gamma_C - \gamma_s) \exp(-\gamma_s t) + (\gamma_f - \Gamma_C) \exp(-\gamma_f t) \right]$$

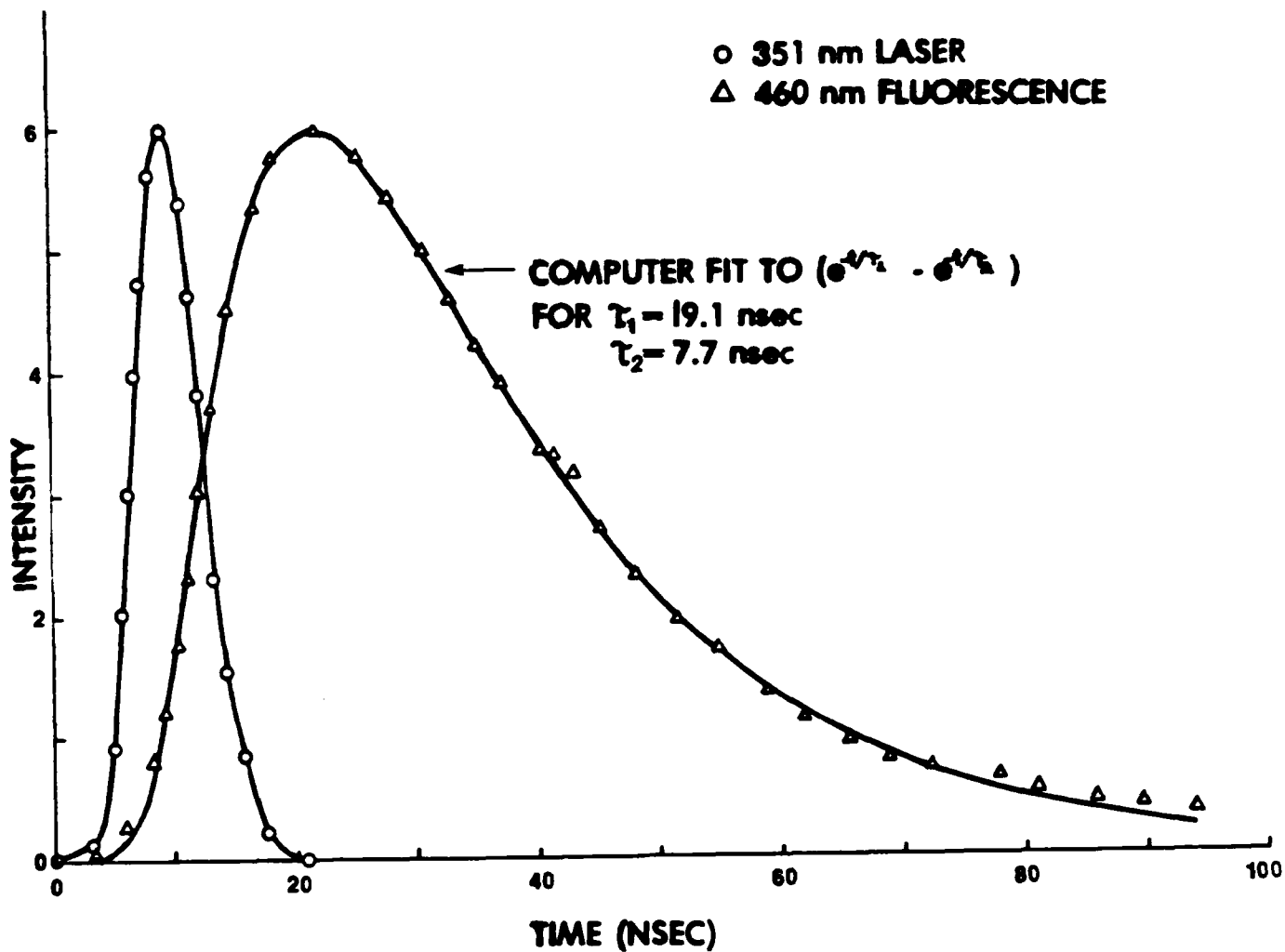
$$G(t) = \Gamma_C (\gamma_f - \gamma_s)^{-1} \left[\exp(-\gamma_s t) - \exp(-\gamma_f t) \right]$$

$$\left. \begin{array}{l} \gamma_f \\ \gamma_s \end{array} \right\} = \frac{1}{2} (\Gamma_B + \Gamma_C) \pm \left[(\Gamma_B - \Gamma_C)^2 + 4\Gamma_{BC} \Gamma_{CB} \right]^{1/2}$$

At low pressures, the two states are not coupled and they each decay with their own characteristic lifetime. At high pressures, the states are tightly coupled and they both decay with the same decay rate which is a linear combination of their individual decay rates.

Figure 2-2 presents oscilloscope traces of the 351 nm exciting laser pulse and the 460 nm broadband fluorescence. The individual points were digitized from Polaroid photographs of the oscilloscope traces. The finite width of the exciting laser pulse must be taken into account in the analysis of the fluorescence data. A computer program was developed which convolutes the exciting laser pulse with a trial fluorescence function and then iteratively determines values of the parameters which give the best fit to the experimental data. Figure 2-2 also shows as a continuous curve the computer fit to the fluorescence function ($e^{-t/\tau_1} - e^{-t/\tau_2}$). The slow time constant gives information on the loss of the C state and the fast time constant gives information on the loss of the B state (quenching + B C transfer).

To determine radiative lifetimes, we measure a set of fluorescence decays as a function of pressure for a mixture with fixed composition. A plot of $1/\tau$ versus P will yield a straight line if bimolecular quenching is dominant. The zero pressure intercept of the straight line fit gives the reciprocal of the



78 01925

Figure 2-2. Oscilloscope Traces Showing the Exciting Laser Pulse and the Subsequent 460 nm Fluorescence. The Individual Points were Digitized from a Polaroid Photograph.

radiative lifetime and the slope of the line gives the effective quenching rate constant for the mixture. Analysis of the fast decay time constants gives the quenching rate constant and radiative lifetime for the XeF(B) state and analysis of the slow decay time constants gives the same information for the C state.

Table 2-1 presents radiative lifetimes obtained from computer fits to the fast and slow decay times of the 460 nm fluorescence for several different mixtures. The uncertainties quoted are the statistical deviation (2 σ) determined from the computer fits. There is considerable scatter and uncertainty especially for the slower C state lifetime. The 5 percent Xe mixtures, deviated from a straight line fit at higher pressures, presumably because termolecular quenching is more important for the higher Xe concentration. The zero pressure intercept for these cases was quite sensitive to the values of the slopes for the quadratic terms. If we only consider the 2.5 percent Xe mixtures which do not exhibit termolecular quenching, the weighted averages of the lifetimes are $\tau_C = 64 \pm 23$ nsec and $\tau_B = 13 \pm 3$ nsec.

Quenching rate constants were obtained by measuring the XeF 460 nm fluorescence decay as a function of concentration of one species while keeping the concentration of all other species fixed. A plot of the reciprocal of the decay time constant versus concentration will give a straight line if bimolecular quenching is dominant. The slope of the straight line fit to the data gives the quenching rate constant for that species. Table 2-2 lists the rate constants determined for most of the constituents used in XeF laser mixtures. The quenching rate constants for the

Table 2-1

XeF Lifetimes Determined from 460 nm Fluorescence

<u>Mixture</u>	<u>τ_C(nsec)</u>	<u>τ_B(nsec)</u>
He + 5%Xe + 0.25%UF ₆	70±52	10.4±2.6
Ne + 5%Xe + 0.25%UF ₆	46±18	8.6±3.0
Ne + 2.5%Xe + 0.12%UF ₆	145±125	13 ±5
He + 2.5%Xe + 0.25%UF ₆	60±25	14 ±5
Ne + 2.5%Xe + 0.25%UF ₆	72±74	9 ±10

For the Three 2.5%Xe Mixtures:

$$\langle \tau_C \rangle = 64 \pm 23 \quad \langle \tau_B \rangle = 13 \pm 3$$

Table 2-2

<u>Quenching Partners</u>	XeF 460 nm Quenching	
	$k_Q^B (\text{cm}^3 \text{sec}^{-1})$	$k_Q^C (\text{cm}^3 \text{sec}^{-1})$
XeF* + He	$1.9 \pm 0.6 \times 10^{-12}$	$\leq 1 \times 10^{-13}$
XeF* + Ne	$\leq 9 \times 10^{-13}$	$\leq 1.1 \times 10^{-13}$
XeF* + Ar	$\leq 1.5 \times 10^{-12}$	$1.1 \pm 0.8 \times 10^{-13}$
XeF* + Kr		$1.5 \pm 1.1 \times 10^{-13}$
XeF* + Xe	$1.46 \pm 0.26 \times 10^{-10}$	$8.0 \pm 0.5 \times 10^{-11}$
XeF* + F ₂	$3.4 \pm 1.9 \times 10^{-10}$	$1.37 \pm 0.15 \times 10^{-10}$
XeF* + NF ₃	$1.7 \pm 0.5 \times 10^{-11}$	$6.5 \pm 1.6 \times 10^{-12}$

XeF(B) state (quenching plus B-C transfer) were obtained by analyzing the fast decay time constants while the quenching rate constants for the C state were obtained by analyzing the slow decay time constants. For several of the rare gases, the scatter in the data is greater than the slope of the straight line fit. For those cases, we have listed the uncertainty in the straight line fits as an upper limit to the quenching rate constants. The data in Table 2-2 show that Xe and F₂ have the largest quenching rate constants for both the B and C states. Quenching of the C state by the lighter rare gases is slow. Quenching of the B state by the lighter rare gases is an order of magnitude faster, but this may be primarily due to collisional transfer to the C state. Note the slower quenching rate constant for both the B and C states by NF₃ compared to F₂.

III. A 490 nm XeF ELECTRIC DISCHARGE LASER*

by

C.H. Fisher, R.E. Center, G.J. Mullaney, and J.P. McDan
Mathematical Sciences Northwest, Inc.
Bellevue, Washington 98004

ABSTRACT

Lasing at 490 nm in the broadband XeF (C 3/2 → A 3/2) transition has been achieved in He/Xe/NF₃ gas mixtures excited by a uv preionized electric discharge. Measurements of the C → A laser spectrum show a bandwidth of approximately 40 nm centered around 490 nm, indicating that the laser should be tunable over a wide spectral region in the visible.

Published by Appl. Phys. Lett. 35, 26 (1979)

*Supported by DARPA under ONR Contract N00014-78-C-0343

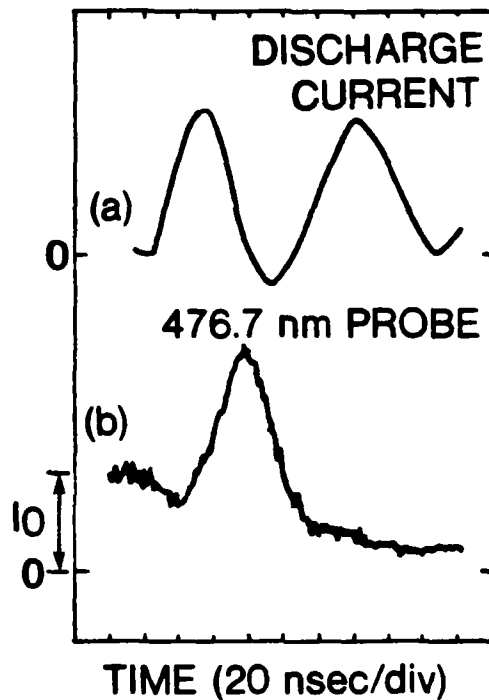
The recent observation of the 480 nm band of XeF, produced by collisional transfer from the XeF B 1/2 state¹ (the upper laser level for the 351 nm XeF laser), has led to attempts to produce a laser on the bound-free C 3/2 \rightarrow A 3/2 transition. Because of the broad spectral width of this band, (~80 nm) the XeF C \rightarrow A transition offers the potential for a high power gas laser tunable over a wavelength range of several tens of nanometers in the visible. Recently, laser oscillation at 480 nm in XeF has been achieved using vacuum ultraviolet radiation to dissociatively excite XeF₂.² We report here lasing on the 480 nm band of XeF excited by a uv preionized electric discharge.

The XeF ionic excited states are efficiently produced both by ion-ion recombination of Xe⁺ with F⁻ and by reaction of F₂ or NF₃ with excited Xe atoms in e-beam or electric discharge excited gas mixtures. Since the C 3/2 state is approximately 0.08 eV lower than the B 1/2 state^{3,4} and since the two states are collisionally mixed by the several atmospheres of rare gas buffer used in these devices,⁴ the C/B population ratio could be as high as 20/1 at room temperature. However the C/B population ratio actually achieved in e-beam or discharge pumped gas mixtures is probably less than the equilibrium value because electron mixing of the B and C states tends to drive their population ratio towards unity.^{2,3} In addition, because of its broad bandwidth and long radiative lifetime, the stimulated emission cross section for the C \rightarrow A transition is 50 to 100 times smaller than that for the B \rightarrow X transition. Thus in order to extract energy efficiently on the lower gain C \rightarrow A transition, it is necessary to carefully choose conditions that will

suppress lasing on the $B \rightarrow X$ transition in addition to favoring formation of the C state.

In order to investigate the conditions favoring lasing, gain measurements were made at several wavelengths in the XeF 480 nm band using a cw argon ion laser as a probe. Figure 3-1 shows a typical oscilloscope trace of the transmitted probe laser intensity at 476.7 nm after two passes through the 50 cm uv preionized discharge. The laser medium exhibits a slight absorption early in the current pulse and then changes into gain at approximately the peak of the current pulse. Similar measurements in pure helium indicate that the late time absorption evident in Figure 3-1 may be due to beam steering effects on the argon ion probe laser and not to actual absorption in the medium. Maximum gain coefficients ranging from 4×10^{-3} to 1×10^{-2} were measured at 457.9, 476.7, 488.0, 496.5, and 514.5 nm. The gain variation as a function of wavelength was approximately a factor of two over the wavelengths quoted with the maximum occurring at 476.7 nm. The highest gains were obtained with a gas mixture of 3 atm He, 3 torr Xe, and 2 torr NF_3 . Reducing the total pressure decreased the amplitude but increased the duration of the gain. The results obtained here are similar to those reported by Hill et al for e-beam excited Ar/Xe/ NF_3 mixtures,⁵ except that the initial absorption is much smaller for our uv preionized discharge which uses helium as the diluent.

Stimulated emission in the 480 nm band was obtained with He/Xe/ NF_3 gas mixtures excited by either of two similar uv preionized discharge devices, having different active lengths. The dimensions of the active



79 02463

Figure 3-1. Oscilloscope Traces Showing the Temporal History of a) the Discharge Current and b) the Transmitted Intensity for the 476.7 nm Probe Laser After Two Passes Through the 50 cm Discharge. The peak gain is $8 \times 10^{-3} \text{ cm}^{-1}$ for a gas mixture consisting of 3 atm He, 3 torr Xe, and 2 torr NF_3 .

discharge volumes of the two devices are 2 cm x 1.5 cm x 50 cm and 3 cm x 1.5 cm x 20 cm. The discharges for these devices were driven by an array of parallel cables, which was pulse charged by a storage capacitor charged to 60 kV. The 50 cm laser utilized a low inductance surface switch⁶ between the cables and the discharge while the 20 cm laser used the laser gas itself as the switch. The surface switch in the 50 cm laser was set to breakdown at 60 kV while the breakdown voltage of the gas in the 20 cm device allowed the cables to charge to approximately 50 kV. The peak current in both devices was approximately 20 kA with a duration of 40 nsec (FWHM) for the 50 cm device and 30 nsec for the 20 cm device.

A high Q optical cavity was formed by sealing dielectrically coated mirrors directly to the discharge cavity. The mirrors were chosen to have high reflectivity at 480 nm and low reflectivity at 351 nm to suppress lasing on the B → X transitions. One of the mirrors had greater than 99.8 percent reflectivity from 440 nm to 500 nm and the other had approximately 1 percent transmission at 460 nm increasing to 1.5 percent at 440 and 480 nm. The rear surface of each mirror was antireflection coated at 352 nm resulting in a reflectivity of less than 15 percent for the full reflector and less than 6 percent for the partial transmitter. Spherical mirrors with 67.5 cm radius of curvature separated by 63 cm were used on the 50 cm laser and 31.7 cm radius of curvature mirrors separated by 31 cm were used on the 20 cm laser. Stimulated emission was not obtained when the mirrors were mounted externally with normal incidence CaF₂ optical windows on the discharge cell.

The temporal histories of the laser and fluorescence emission obtained with the 50 cm device are compared in Figure 3-2. These traces were taken using two broadband interference filters in front of a calibrated photodiode which was placed about 40 cm from the output mirror. A mirror with maximum reflectivity at 350 nm was used to filter out any amplified spontaneous emission at 351 and 353 nm. The fluorescence emission trace was taken with the same conditions as for the laser emission, except that the cavity mirrors were mounted externally so that no lasing took place (blocking the rear mirror under these conditions only reduced the photodiode signal by a factor of two). In addition to the factor of 60 increase in intensity obtained with the internal mirrors, the optical pulse is delayed by approximately 40 nsec and broadened by about 50 nsec. This time delay is the time required for the cavity intensity to build up above threshold. From the decay time of the laser emission, it is estimated that the losses per pass are approximately 3 percent for the 50 cm device and 2 percent for the 20 cm device.

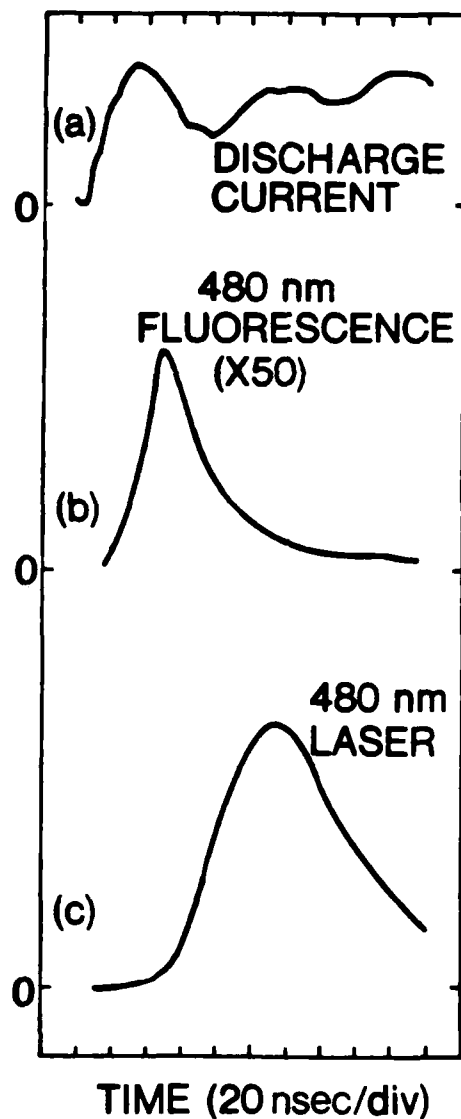
The maximum laser emission was obtained with a gas mixture consisting of He + 0.12% Xe + 0.09% NF₃ at 3 atm total pressure. By integrating the area under the calibrated photodiode trace and including the appropriate filter transmissions, an estimated energy of 50 J was obtained in a 70 nsec pulse with the 20 cm laser and approximately one third as much with the 50 cm laser. The beam divergences for the relatively short radius of curvature confocal cavities used in these experiments were approximately 40 milliradians (half angle) for the 20 cm laser and 10 milliradians for the 50 cm laser. Thus the brightness (photons cm⁻²

sec⁻¹ steradian⁻¹) is actually lower for the 20 cm laser even though the output energy is higher. These divergences are consistent with the predictions of 45 and 20 milliradians calculated from the formula

$$\theta = \sqrt{2} (a/d)$$

derived by Bridges for a multimode confocal cavity of diameter 2a and mirror spacing d.⁷

In Figure 3-3 spectrally resolved measurements of the laser emission are presented which show a bandwidth of 25 nm centered at 490 nm. The broadband laser spectrum exhibited several discrete gaps which probably arise from absorption lines due to species present in the discharge, e.g., excited Xe* and Xe₂* molecules and Xe⁺. This broadband spectrum indicates that the laser should be tunable over a wavelength range of several tens of nanometers. Plates taken of the fluorescence emission with the mirrors removed show a broad continuum emission extending over approximately 100 nm and exhibiting a few discrete absorption and emission lines. Surprisingly, this spectrum does not show the broad peak at approximately 460 nm reported by Brashears and Setser, but more closely resembles their low pressure spectrum.⁴ This could imply that the C state is formed in high vibrational levels which are not fully relaxed under our conditions (3 atm He). An alternate explanation is that the 460 nm XeF spectrum obtained by Brashears and Setser with 200 torr of Kr buffer actually contains contributions from excited triatomic XeKrF* molecules, which are expected to emit in this spectral region.⁸



79 02464

Figure 3-2. Time Correlated Oscillograms Showing a) the Discharge Current, b) the 480 nm Fluorescence With an External Optical Cavity, and c) the 480 nm Laser With the Same Optical Cavity Mounted Internally. Note that the stimulated emission reaches a maximum significantly later than the fluorescence due to the cavity buildup time.

It is evident from the results of this work that the performance of the present device is limited by the low value of the small signal gain combined with the short time available for buildup of stimulated emission. This is illustrated by the photodiode trace in Figure 3-3, which shows that the 480 nm lasing reaches its peak when the excitation pulse is essentially over. The performance of the C → A laser could be enhanced by extending the duration of the pumping pulse to allow the cavity intensity to build up to saturation. Alternatively more efficient extraction of energy might be achieved from the present device by injecting a signal into a regenerative amplifier in order to saturate the medium before the gain terminates. Efforts to improve the laser performance using these techniques are presently underway.

Since the XeF excited states are efficiently produced by discharge excitation the C → A transition has the potential for an efficient high power gas laser tunable over a bandwidth of approximately 40 nm in the visible. In order to realize this potential, a method will have to be found to saturate the C → A transition in order to compete effectively against excited state losses through the higher gain B → X transition.

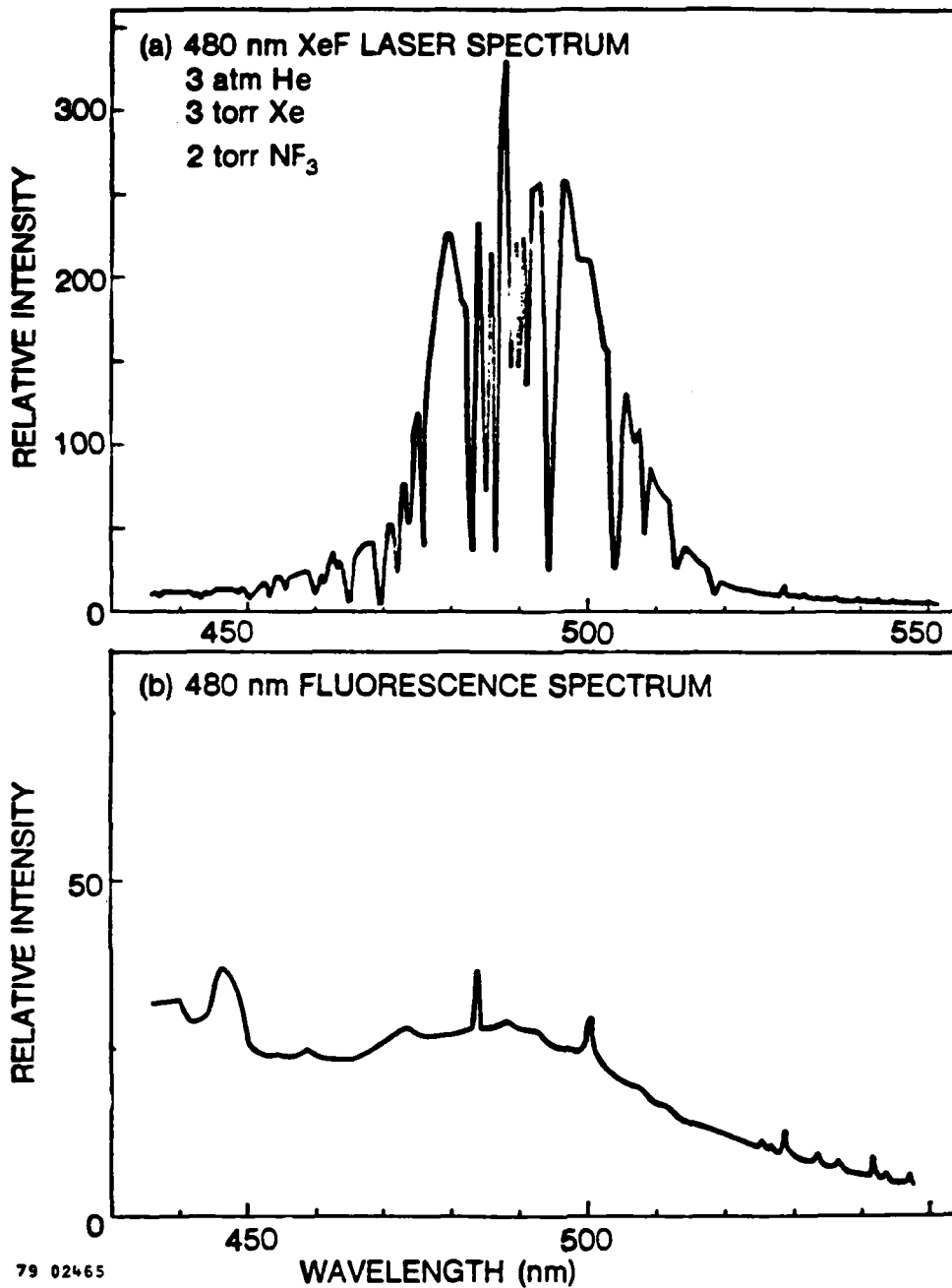


Figure 3-3. Densitometer Tracings of Plates Taken of a) the XeF 480 nm Stimulated Emission Spectrum and b) the 480 nm Fluorescence Spectrum Obtained With the Mirrors Replaced by CaF₂ Windows. The spectra have been corrected for a factor of two increase in film sensitivity from 500 to 430 nm.

REFERENCES

1. C.H. Fisher and R.E. Center, J. Chem. Phys. 69, 2011 (1978).
2. W.K. Bischel, H.H. Nakano, D.J. Eckstrom, R.M. Hill, D.L. Huesteis, and D.C. Lorents, "A New Blue-Green Excimer Laser in XeF", (to be published).
3. D. Kligler, H.H. Nakano, D.L. Huestis, W.K. Bischel, R.M. Hill, and C.K. Rhodes, Appl. Phys. Lett. 33, 39 (1978).
4. H.C. Brashears and D.W. Setser, Appl. Phys. Lett. 33, 821, (1978).
5. R.M. Hill, P.L. Trevor, D.L. Huestis, and D.C. Lorents, Appl. Phys. Lett. 34, 137 (1979).
6. W.J. Sarjeant, A.J. Alcock, and K.E. Leopold, IEEE J. Quantum Electron, QE-14, 177 (1978).
7. W.B. Bridges, Appl. Opt., 14, 2346 (1975).
8. M. Krauss (private communication).

IV. MULTIPASS AMPLIFICATION AND TUNING OF THE
BLUE-GREEN XeF C → A LASER*

by

C.H. Fisher, R.E. Center, G.J. Mullaney, and J.P. McDaniel
Mathematical Sciences Northwest, Inc.
Bellevue, Washington 98004

ABSTRACT

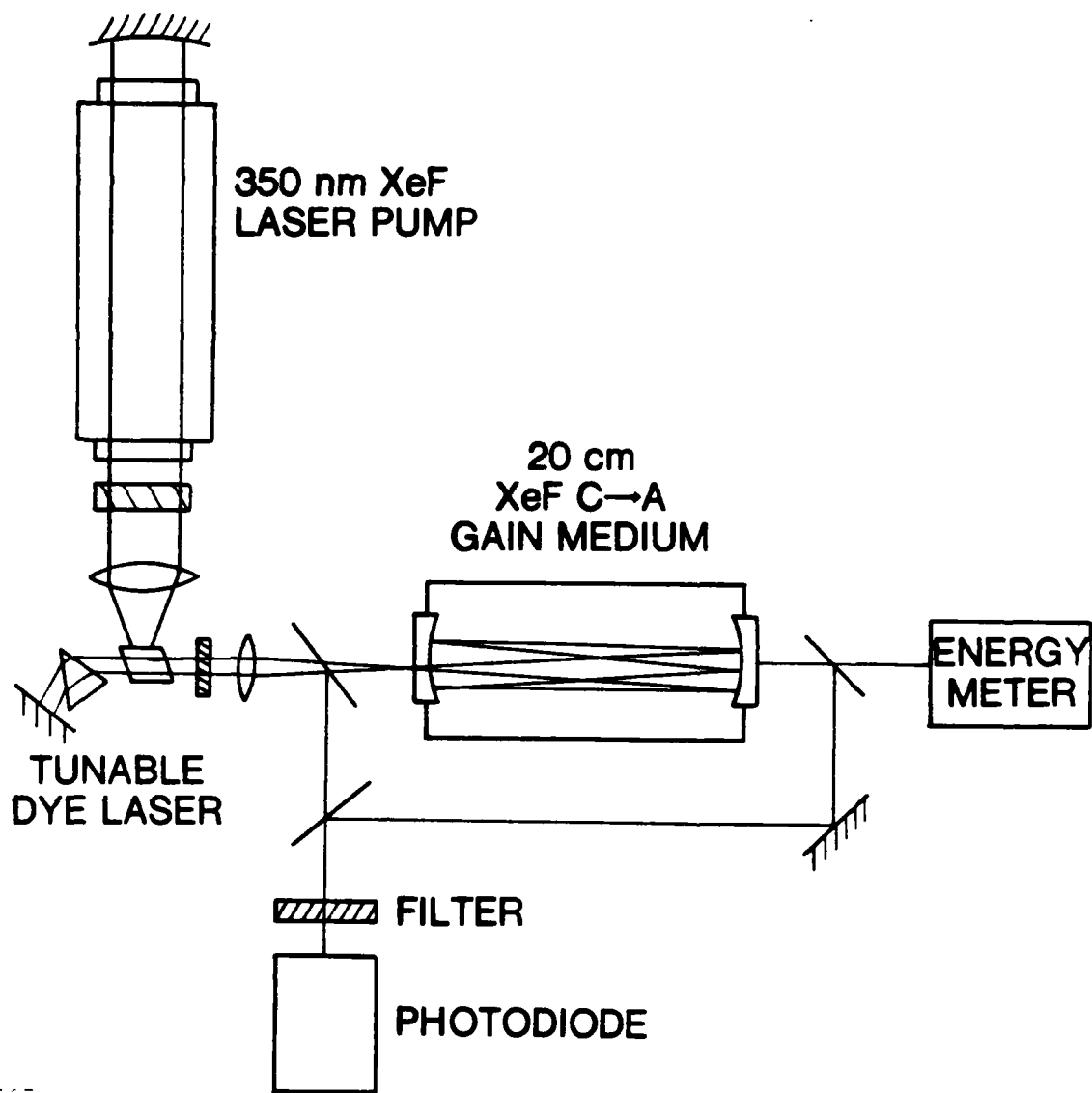
The output energy from a uv preionized discharge excited XeF C → A laser has been increased by two orders of magnitude by injecting a dye laser pulse into the C → A oscillator cavity. Output energies greater than 4 mJ with a spectral bandwidth of approximately 3 nm have been measured. By tuning the injected dye laser pulse, the output from the C → A laser was tuned from 460 to 515 nm.

Published by App. Phys. Lett. 35, 901 (1979)

*Supported by DARPA under ONR Contract N00014-78-C-0343

Recently several groups¹⁻³ have reported lasing on the broadband C-A transition in XeF at 480 nm. This transition is of interest because of its visible wavelength, and the fact that it is potentially tunable over several tens of nanometers. In the earlier experiments lasing was achieved using both optical dissociative excitation² of XeF₂ diluted in Ar and uv preionized discharge excitation of He/Xe/NF₃ mixtures.^{1,3} The relatively low values of small signal gain^{1,4} coupled with the short time available for the buildup of stimulated emission in the uv preionized discharge limit the output energy of the discharge excited lasers to several tens of microjoules. It is evident that injecting a light pulse having a much higher intensity than the C-A spontaneous emission would decrease the time to reach threshold and significantly improve the laser performance. In addition, the wavelength of the C-A laser could then be tuned by simply tuning the injected signal. This paper describes such experiments to improve the output energy and to tune the XeF C-A laser by injecting a dye laser pulse into the cavity.

Figure 4-1 shows the experimental set up. The injected signal is provided by a tunable dye laser pumped by a 350 nm XeF laser operating on the "normal" B-X transition. The 10 mJ output from the pump laser was focussed to a line on the inside face of the dye cell. The dye laser was used both broadband and tuned by the addition of two prisms to the cavity. The dye 7-diethylamino 4-trifluoromethylcoumarin (2.5×10^{-3} M in p-dioxane) was tuned from 465 to 515 nm and 7-diethylamino 4-methylcoumarin (2.5×10^{-3} M in ethanol) was used from 445 to 465 nm. The dye laser beam was



79 02897

Figure 4-1. Schematic Diagram of the Multipass Amplifier Experiment.

enlarged by a five times expanding telescope, then focussed into the C-A laser through a 1 mm hole in the high reflectivity mirror forming one end of a high Q optical cavity. The dye laser was injected off axis so that the refocussed spot walked around the mirror and did not return to the entrance hole for many round trips.⁵ The pattern of overlapping spots on the output mirror described an annulus, and covered approximately one third of the entire gain volume. The mode pattern of the amplified emission from the C-A laser was the same as that produced by the dye laser alone.

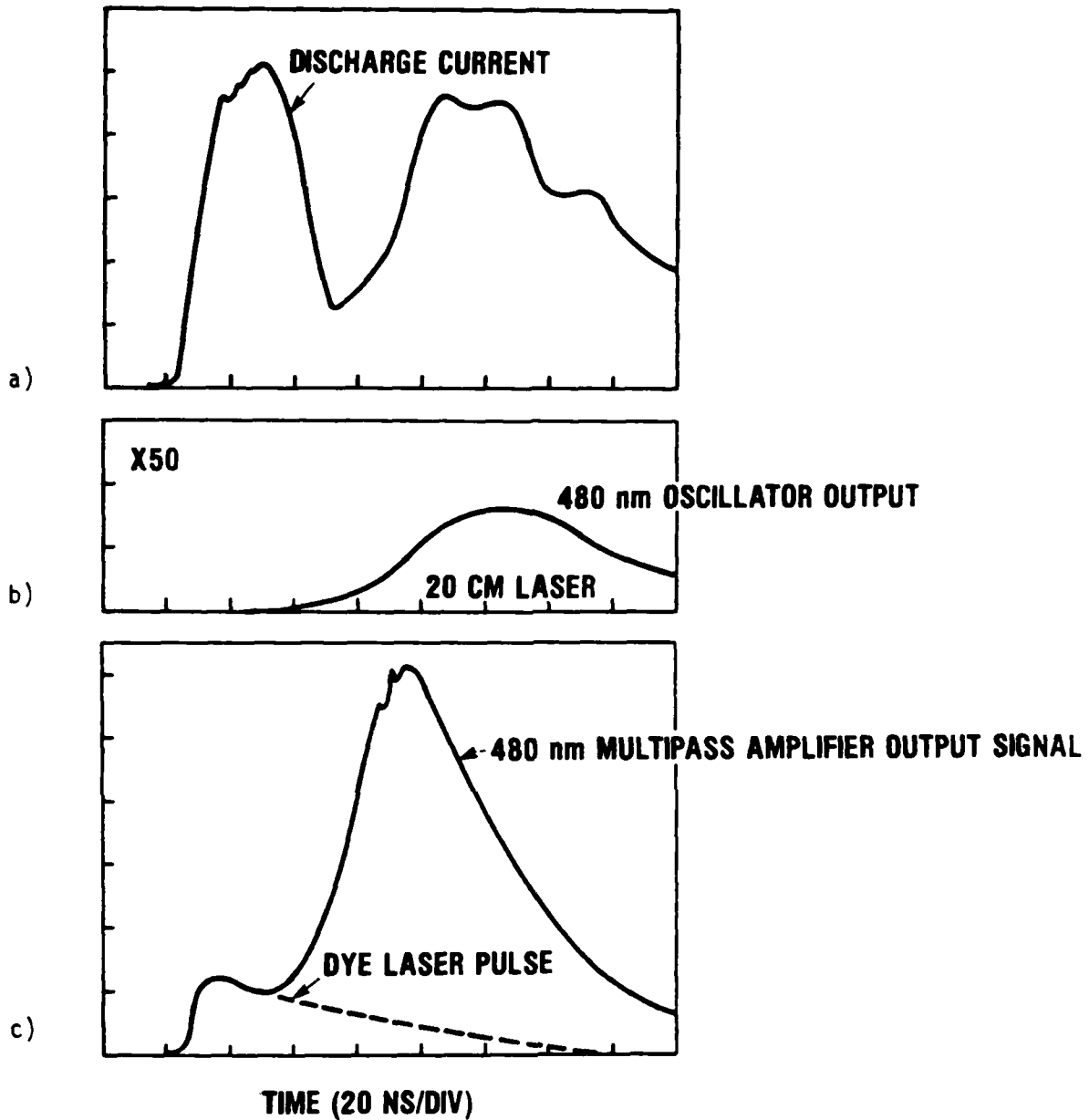
Since the dye laser is injected off axis to keep it from escaping back out the entrance hole after three round trips, the beam traverses the cavity many times before retracing its path and therefore does not establish a standing wave in the cavity. As a result this configuration can be thought of as a multipass amplifier in which a small fraction of the energy is extracted each time the amplified beam returns to the output mirror.

The XeF C-A laser was excited by a uv preionized discharge having an active volume of 20 cm x 3 cm x 1.5 cm. This laser was more fully described in our previous paper¹ and will only be briefly described here. The pulse forming network, consisting of an array of eight cables 2.4 m long, was pulse charged by a 25 nF capacitor charged to 60 kV (stored energy = 45 J). The gas mixture consisted of 3 atm He + 3 torr Xe + 2 torr NF₃. Two internal mirrors separated by 31 cm formed the optical cavity. Two sets of mirrors with different output coupling and different radii of curvature were employed. One set of

mirrors had a 67.5 cm radius of curvature and the other set had a 217 cm radius of curvature. The mirrors were coated for high reflectivity at 480 nm and high transmission at 350 nm to discriminate against the high gain B-X transition. Both sets of mirrors had a maximum reflector with $R_{480} > 0.995$ and $T_{350} > 0.85$ and the output couplers had $T_{480} = 0.01$, $T_{350} = 0.94$ and $T_{480} = 0.02$, $T_{350} = 0.94$ for the 67.5 cm and 217 cm radius of curvature mirrors, respectively. Uncoated Pyrex beam splitters sampled the injected and amplified beams and a wide bandwidth interference filter in front of the vacuum photodiode rejected 350 nm light. The 480 nm broadband output energy was measured with a pyroelectric energy meter (Gen. Tech. ED 200).

Figure 4-2 presents oscillograms of the discharge current and the output of the XeF C-A laser both with and without injection of the dye laser pulse. The transmitted dye laser pulse appears just prior to the amplifier output and the time dependence of the dye laser pulse transmitted by the XeF laser oscillator cavity is shown by the dotted curve in Figure 4-2c. Since the round trip time in the amplifier cavity is 2 nsec the 70 nsec decay of the transmitted dye laser pulse indicates that the dye pulse was trapped for approximately 30 round trips. The output energy was not sensitive to timing variations of ± 10 nsec as long as the dye laser pulse was injected before the first peak of the current pulse.

The energy of the injected dye laser pulse measured in front of the C-A laser input mirror was typically 0.5 to 1 mJ. The transmitted dye laser energy measured without firing the C-A laser was 0.1 mJ



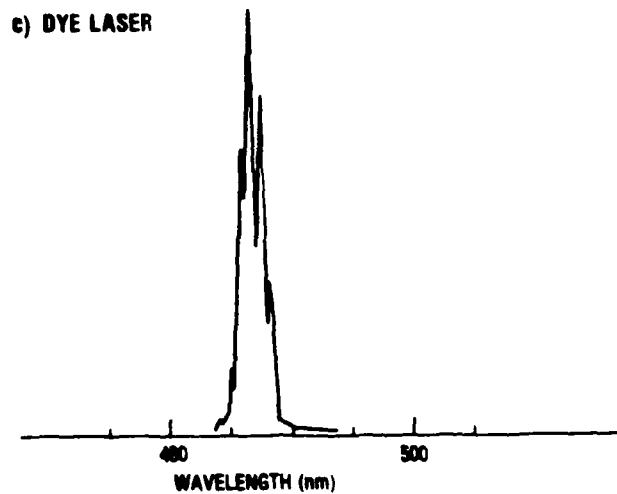
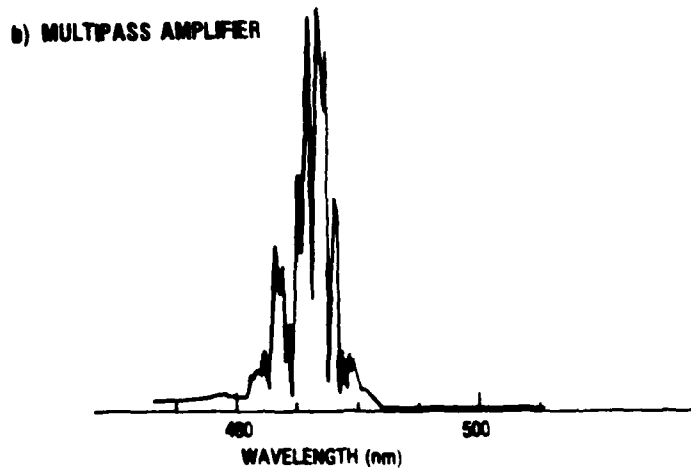
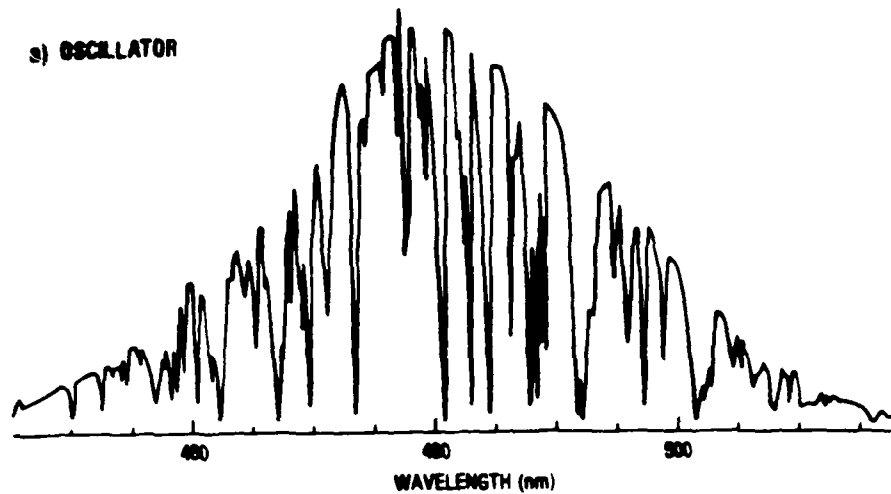
79 02899

Figure 4-2. Oscilloscope Traces Showing the Temporal Dependence of a) the Discharge Current, b) the XeF C→A Laser Output Without Dye Laser Injection and c) the C→A Laser Output With Dye Laser Injection. The dashed curve shows the temporal dependence of the transmitted dye laser pulse obtained without firing the C→A laser.

or less. Output energies of greater than 4 mJ from the multipass amplifier have been obtained with the 2 percent output coupler and the temporal behavior is similar to that presented in Figure 4-2c. Photodiode measurements of the radiation coming back out of the 1 mm entrance hole indicate that the beam escaping from the hole after about 30 round trips has an energy greater than the injected pulse (0.5 to 1 mJ). In fact, the tuning experiments described below had to be discontinued when the amplified beam damaged the mirror substrate at the input hole.

Figure 4-3 shows a spectrum of the C-A oscillator without dye laser injection, the C-A laser with dye laser injection, and the injected dye laser itself. No effort was made to narrow the bandwidth of the prism tuned dye laser which had a bandwidth of about 3 nm. The structure in the dye laser spectrum probably results from etalon effects due to the dye cell windows. As is evident from Figure 4-3b, this structure is preserved in the multipass amplifier spectrum except for gaps due to absorption lines present in the XeF C-A gain medium. These absorption lines are visible in the oscillator spectrum of Figure 4-3a. It is also apparent from Figure 4-3b that weak emission in the wings of the dye laser spectrum is amplified in the C-A laser.

Experiments were then made to tune the output of the XeF C-A amplifier by tuning the dye laser with two prisms. Figure 4-4 presents the results of these tuning experiments. It was found that the output could be tuned from 460 to 515 nm with energies in excess of 1 mJ. No effort was made to avoid the absorption features evident in the oscillator spectrum, Figure 4-



79 03148

Figure 4-3. Spectra of the Stimulated Emission From a) the XeF C⁺A Oscillator, b) the C⁺A Multipass Amplifier, and c) the Injected Dye Laser. These spectra were obtained by densitometering plates taken with a 0.5 meter spectrometer and have been corrected for a factor of two decrease in film sensitivity from 430 to 500 nm.

3a. The transmission of the output mirror for the C-A laser is also plotted in Figure 4-4. Surprisingly significant output was obtained at wavelengths for which the mirror transmission is quite high implying that higher output coupling in the center of the C-A band might yield higher output energies. A set of mirrors with an output coupler having 2 percent transmission at 480 nm was then tried. These experiments yielded greater than 4 mJ both at 490 and 470 nm until the input mirror was damaged by the amplified beam.

Although both the optical configuration and the discharge characteristics are far from ideal, these experiments show that the performance of the XeF C-A laser can be substantially improved by injecting a signal having a much higher intensity than the background spontaneous emission. Further improvements could be realized by injecting the dye laser beam so that it extracts energy from the entire gain volume. In addition the tuning range of 460 to 515 nm was probably limited by the mirror coatings and can likely be extended with the proper choice of output coupling.

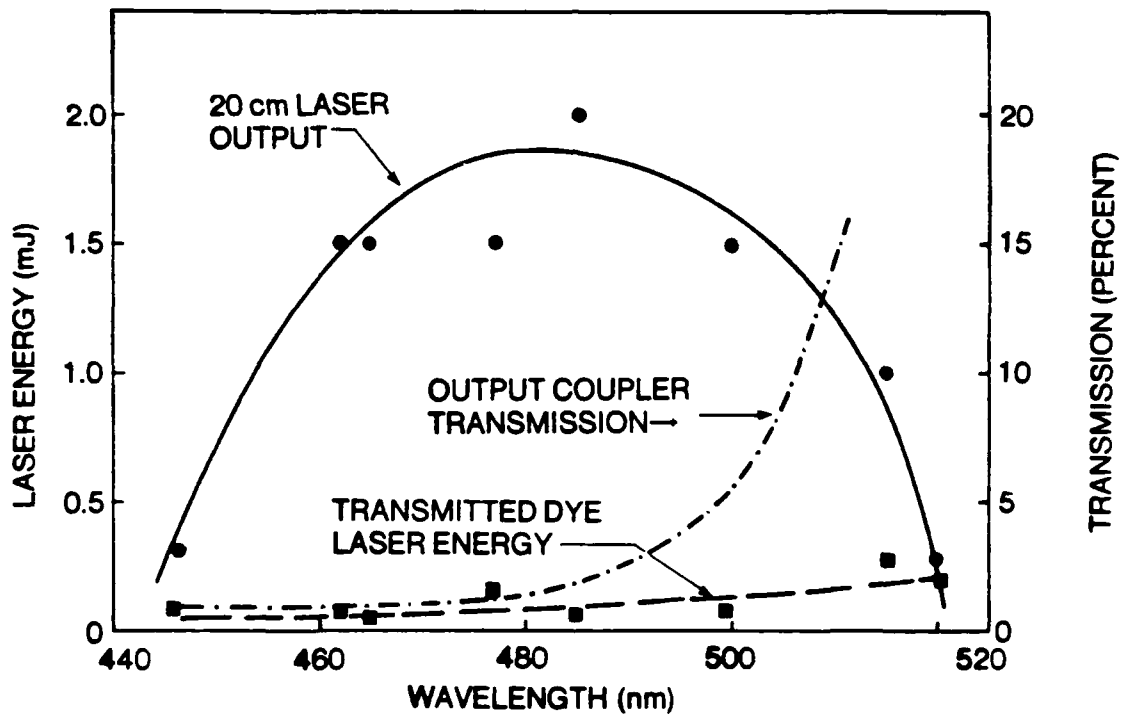


Figure 4-4. Laser Energy As a Function of Wavelength for the XeF C→A Multipass Amplifier. The dye laser energy transmitted by the cavity without firing the C→A laser is also shown. The output mirror used in these experiments had one percent transmission at 460 nm.

REFERENCES

1. C.H. Fisher, R.E. Center, G.J. Mullaney, and J.P. McDaniel, Appl. Phys. Lett. 35, 26 (1979).
2. W.K. Bischel, H.H. Nakano, D.J. Eckstrom, R.M. Hill, D.L. Huestis, and D.C. Lorents, App. Phys. Lett. 34, 565 (1979).
3. R. Burnham, Appl. Phys. Lett. 34, 48 (1979).
4. R.M. Hill, P.L. Trevor, D.L. Huestis, and D.C. Lorents, Appl. Phys. Lett. 34, 137 (1979).
5. D. Herriot, H. Kogelnik, and R. Kompfner, Appl. Opt. 3, 523 (1964).

V. E-BEAM PUMPING OF THE XeF C-A LASER

The prospect of developing a high-power gas laser potentially tunable over a large region of the visible spectrum has generated continuing interest in the blue-green excimer laser based on the C-A transition in XeF. Various excitation techniques have resulted in laser oscillation on this bound-free transition, including photolysis of XeF₂,^{1,2} electric discharge excitation of He/Xe/NF₃ mixtures,³⁻⁵ and high current density, short-pulse e-beams in Ar/Xe/NF₃ mixtures.⁶ The observation of laser emission in the afterglow of short-pulse e-beams was consistent with earlier gain measurements under similar conditions.⁷

The C-A laser is characterized by a small stimulated emission cross section ($\sigma \sim 10^{-17}$ cm²),⁷ a fairly short collisional lifetime (≤ 25 ns),⁸ and a saturation intensity of the order of 1 MW/cm².⁹ Because of the limited magnitude of the small signal gain observed in previous experiments and the short persistence time of the excited species, the laser performance was limited due to insufficient time for buildup to saturation.

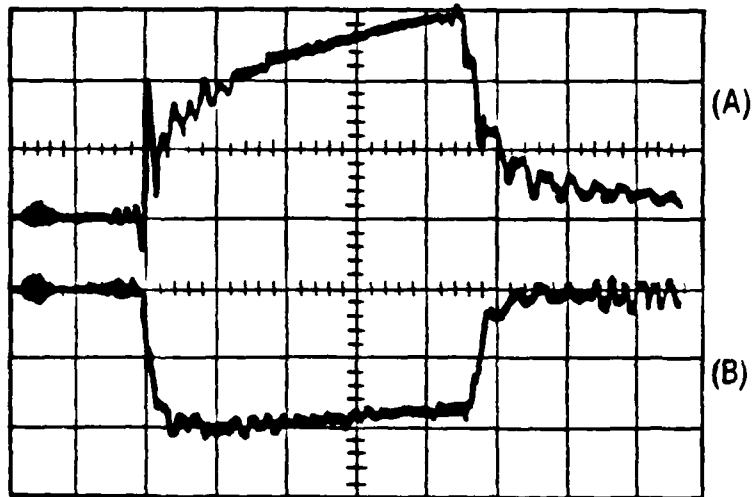
In this paper we report results of laser experiments using direct excitation by a low current density (≤ 10 amps/cm²), long pulse duration (≤ 1 μ sec) e-beam. Oscillation on the C-A transition was observed during the pumping pulse, although the laser did not saturate by the end of the pulse due to the low magnitude of the net gain. We have measured the net gain on the C-A transition for a variety of gas mixtures; the highest gains measured were 5×10^{-4} cm⁻¹

in both 0.25% Xe/0.12% NF₃ in Ne and 0.25% Xe/0.12% F₂ in Ar. A Kr/Xe/F₂ mixture (for which the net gain was not measured) exhibited the best laser performance. Fluorescence and laser emission spectra show numerous absorption features as found previously with discharge excitation.³⁻⁵ The number of absorption features decreased in Kr-based mixtures.

Apparatus

The broad area, cold cathode electron gun used in these experiments was connected to a three-stage Marx generator with 0.9 μ f per stage (two 75 kV, 1.8 μ f capacitors in series). When charged to 120 kV the total stored energy in the Marx was 19.4 kJ, and the electron gun produced e-beam pulses at approximately 340 kV for up to 1 μ sec duration. The electron gun cathode measured approximately 5 cm wide by 1 m long and consisted of three 0.3 mil tantalum blades mounted 3 cm apart within an electrostatic focusing structure. This assembly was supported by a vacuum housing coupled to the photolytic chamber via a conventional Hibachi type foil support structure.

Electron gun diagnostics included measurement of the total gun current and voltage at the output of the Marx. The time resolved gun current was measured using a current transformer (Pearson Electronics, Inc. Model 3025). The voltage was measured using a fast (~ 10 nsec risetime) resistive divider adapted from a design described elsewhere. Typical current and voltage waveforms for the electron gun are shown in Figure 5-1. A charging voltage of 120 kV was used. The sensitivity for the current trace was 4×10^3 amps/division, and the sensitivity for the voltage



200 nsec/div

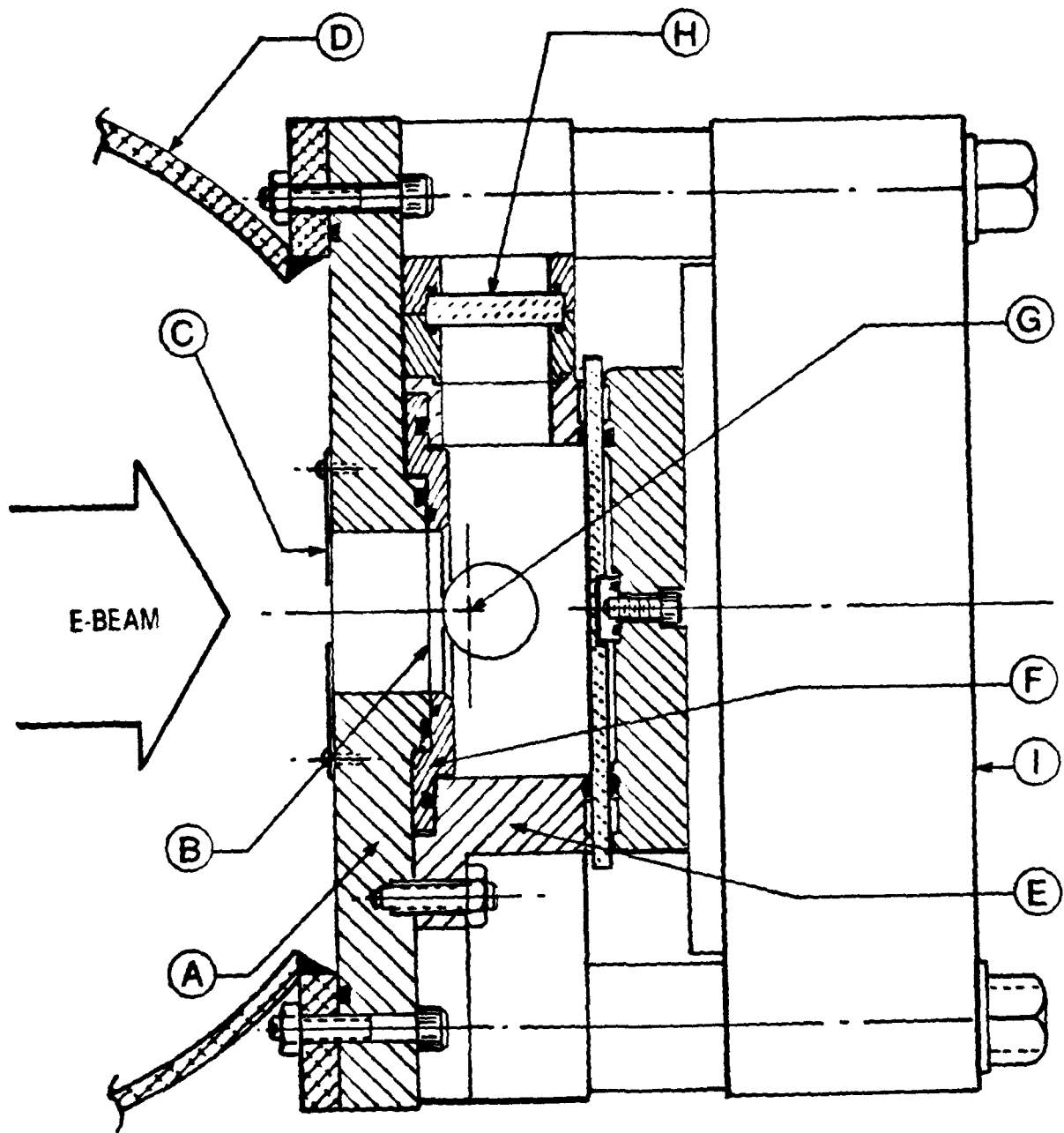
79 03449

Figure 5-1. Electron Gun Current and Voltage Waveforms. (A) Current trace measured at the output of the Marx. Vertical sensitivity is 4×10^3 amps/division. (B) Voltage trace measured at the output of the Marx by the resistive voltage divider. Vertical sensitivity is 1.7×10^5 V/division.

trace was approximately 1.7×10^5 V/division. The measured peak voltage for the 900 nsec duration pulse was 3.4×10^5 V.

A cross sectional view of the laser chamber used for most room temperature experiments is shown in Figure 5-2. The chamber was constructed entirely of aluminum with an interior volume of approximately 10 l. The interior surfaces were originally highly polished for a separate experimental application. However, for use as an XeF chamber, these surfaces were coated with 2 mil Teflon tape to help suppress formation of parasitic oscillations on the XeF (B-X) transitions. A series of 1 inch diameter stainless steel apertures evenly spaced along the 1 m excitation length was also used to suppress parasitic oscillations. Vacuum seals within the chamber were made using grease-free Viton O-rings which were shielded from contact with the e-beam. The chamber was equipped with viewing ports for measurement of net gain or observation of fluorescence along the optical axis through MgF_2 windows. The optical axis was located 1.2 cm from the e-gun foil (typically 1.3 or 2 mil aluminum).

Quantitative measurements of e-beam uniformity and energy deposition were carried out in air using both calorimeter arrays and a Faraday cup. Results obtained using the two techniques agreed to within approximately 10 percent and showed that a peak e-beam current density, j_{eb} , of 12 amps/cm² was attainable along the optical axis for an anode-cathode spacing of 5 cm and e-beam pulse durations greater than 700 nsec. Over the 1 inch dimension defined by the diameter of the cavity mirrors used in the oscillator experiments,



79 03450

Figure 5-2. Cross Sectional View of the XeF Laser Chamber.
 (A) Hibachi Structure, (B) E-gun foil,
 (C) Strongback, (D) E-gun Vacuum Housing,
 (E) Photolytic Chamber, (F) E-gun foil
 Retaining Ring, (G) Optical Axis, (H) MgF_2 Window.

j_{eb} decreased to 10 amps/cm². Variations in energy deposition along the optical axis were not greater than ± 10 percent. Increasing the anode-cathode spacing to 5.5 cm decreased j_{eb} by ~ 10 percent. As a result, the average current density throughout the ~ 0.5 l active volume was taken to be ~ 10 amps/cm² for anode-cathode spacings of 5.0 or 5.5 cm and pulse durations greater than 700 nsec.

The 1 m laser chamber was operated at pressures up to a maximum of 5 atm using Ne diluent in the gas mixture. Under these conditions the optical axis was located at approximately 75 percent of the maximum energy deposition predicted by electron scattering codes. In the case of Ne diluent, the energy deposition function was slowly varying over the dimensions of the active volume. Hence, the XeF gain distribution normal to the optical axis should be relatively insensitive to changes in the average energy deposition, and the effect of different pressures of Ne mixtures should manifest itself principally via changes in the rates of the kinetic processes. While mixtures containing Ar and Kr diluents were used at stopping powers equivalent to 5 atm Ne, the energy deposition varied considerably over the dimensions of the active volume so that the gain distribution is in principle more sensitive to pressure due to both changes in the average energy deposition as well as in the kinetic rates.

If the B to C state population ratio is determined by heavy particle collisions and not electron mixing, then it may be possible to increase the population of the lower lying C state by cooling the laser gas mixture. Because the C-A transition does

not suffer from the problem of lower level buildup, reducing the temperature would not limit the energy extraction as it does on the B-X transition. Consequently, for some experiments the 1 m laser chamber was replaced by a 0.5 m chamber designed to cool the gas mixture. A schematic diagram of this chamber is shown in Figure 5-3. The e-beam foil was in this case mounted directly onto the cooled chamber so that the entire assembly was thermally isolated from the electron gun by means of high vacuum. The cooled chamber is mechanically supported by an aluminum outer shell using stiff stainless steel bellows and thin wall stainless steel brackets. Both the stainless steel chamber and foil support structures were directly cooled via metal coils containing the cryogenic fluid. The fluid was also pumped through ceramic feedthroughs directly to the metal discharge anode. Since the chamber was not operated in a discharge mode in these experiments, the anode served primarily to promote rapid cooling of gas mixtures. The use of a rubber O-ring seal between the chamber and the foil restricted cooling temperatures to $\sim -30^{\circ}\text{C}$ at the 5 atm maximum pressure used with Ne rich mixtures. Frosting of the cold inner window was avoided by an auxiliary high vacuum system connected to the space between the warm and cold window assembly.

The optical axis of the cooled chamber was located approximately 2.5 cm from the foil. This location was somewhat closer to the predicted maxima of the energy deposition functions (~ 80 percent of the maximum for Ne) for the pressures used than was the case with the 1 m chamber. The total energy deposited per cm^3 of active volume was most likely lower using the cooled chamber, however, due to spreading of the e-

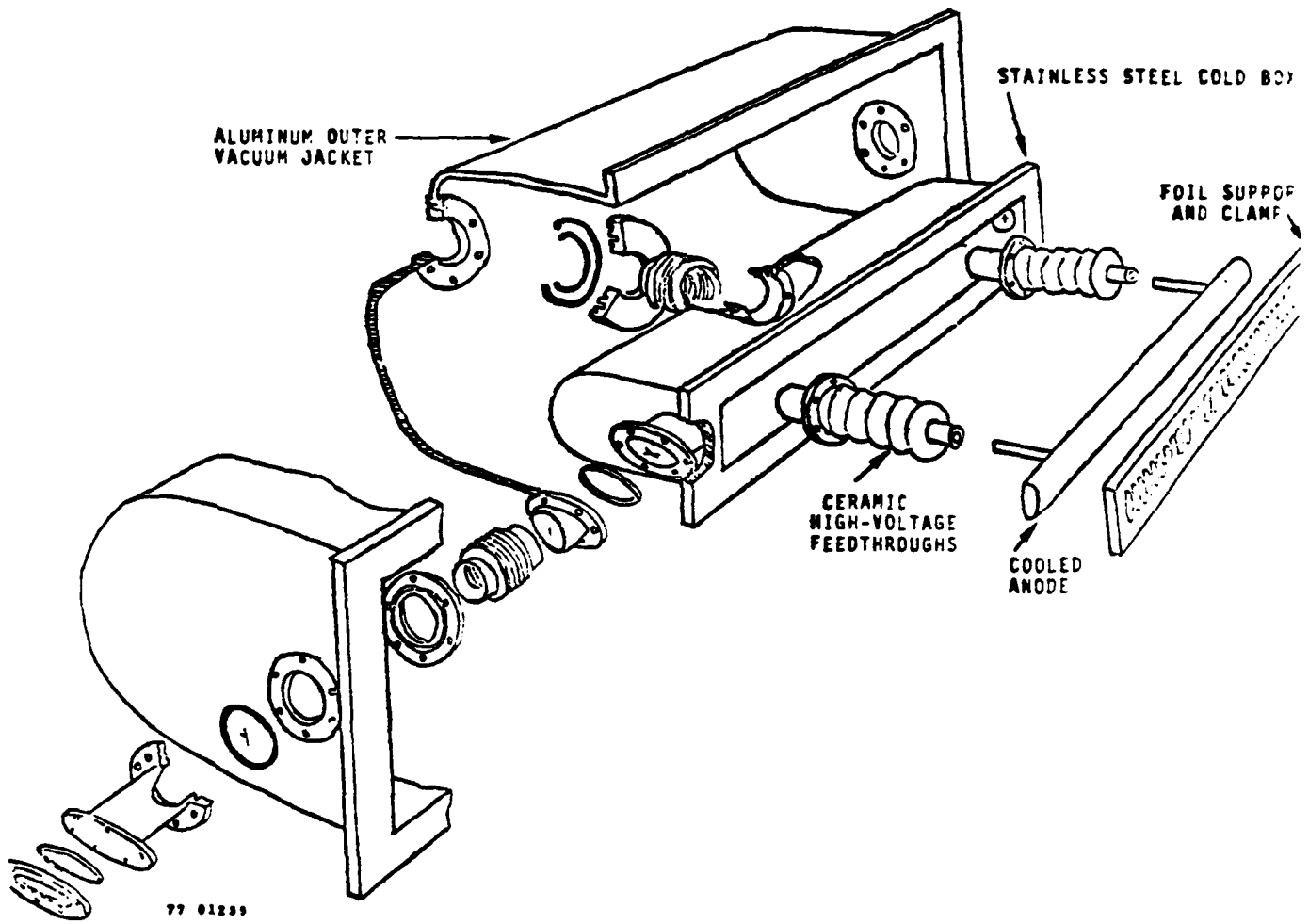


Figure 5-3. 0.5m Cooled XeF Laser Chamber.

beam over the approximate 10 cm drift region between the e-gun anode and the foil. The effect of beam spreading was not investigated.

Gas mixtures were prepared in F_2 passivated steel or aluminum cylinders using Ne (99.996%), Ar (99.998%), Kr (99.995%), NF_3 (98%), and F_2 (98%) directly from commercial cylinders without further purification. The laser chambers were initially passivated over a period of days using periodically renewed 1 atm fills of a mixture of 2 percent F_2 in He. The chambers were repassivated following exposure to the atmosphere during various maintenance or repair procedures.

A schematic diagram of the apparatus used to probe the gain on the XeF C-A band is shown in Figure 5-4. The beam from an argon ion laser tuned to either 488.0 or 514.5 nm (nominal 1 W single line output) was used to probe the e-beam excited gas medium in a two pass arrangement and was monitored by a calibrated ITT type F4000 S-5 photodiode operated at 2500 V. The probe beam was chopped by a rotating disk to avoid saturating the photodiode. Filters were used both to suppress laser oscillation on the B-X transitions and to isolate the spectral region being probed. Signals due to spontaneous emission from the C-A band were reduced to a negligible level by locating the detector 5 m from the photolytic chamber and restricting the detector aperture. The photodiode signal was used to generate a gate pulse to the delay unit which synchronously fired the e-beam and triggered the oscilloscope.

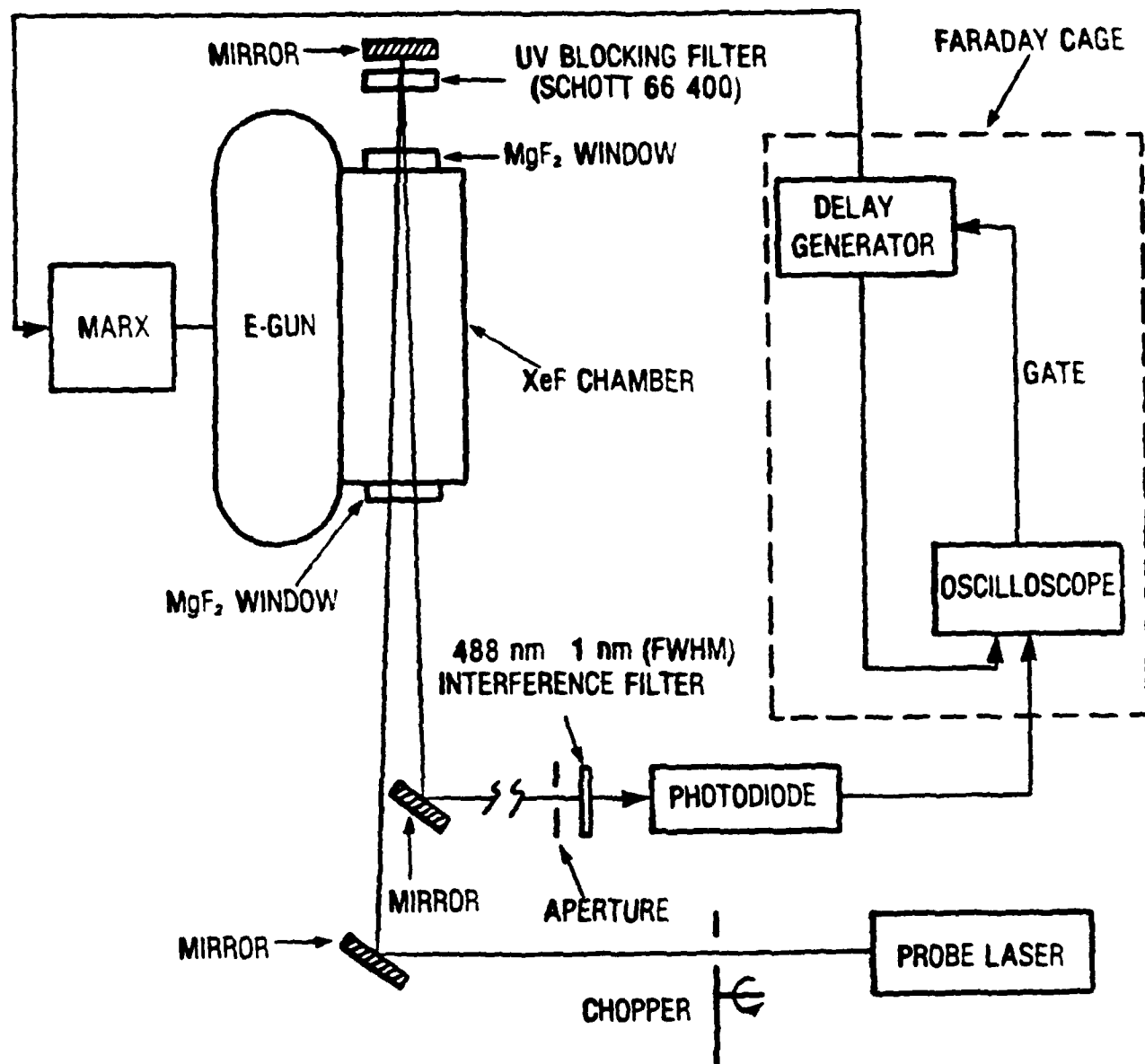
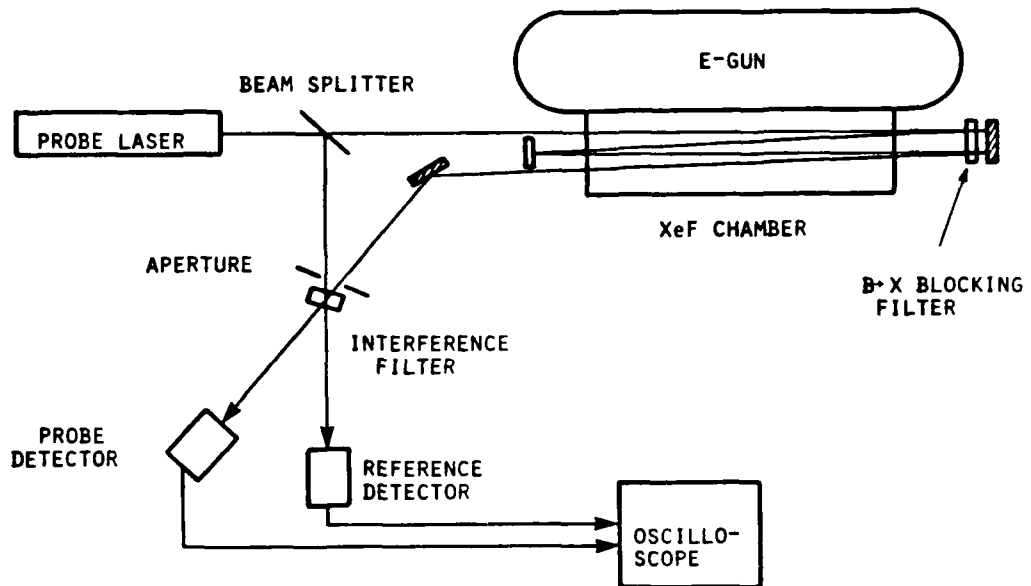


Figure 5-4. Diagram of Apparatus Used for XeF Gain Measurements. The photodiode signal is used to generate a gate pulse to the pulse delay unit which synchronously fires the e-beam and triggers the oscilloscope. The shielded photodiode is located approximately 5 m from the XeF chamber.

For experiments which required the use of the cooled, 0.5 m chamber, the optical arrangement needed to be modified to a 4 pass configuration to measure the net gain with a sensitivity comparable to data obtained using the 1 m chamber. For gain experiments using the 4 pass configuration with the cw laser probe, the low signal intensity required substitution of an RCA type 1P28 photomultiplier in place of the usual vacuum photodiode. The 1P28 was operated at 600 V.

For gain experiments in which Ar was the diluent, a flashlamp pumped, grating tuned dye laser (Phase-R Model DL-1200 uv) was used to verify that the cw measurements were not influenced by argon ion absorption within the e-beam excited medium. A diagram of the apparatus modified to permit pulsed dye laser measurements of net gain is shown in Figure 5-5.

A standard dual beam approach was used whereby the ratio of probe to reference beam intensities was compared before and during e-beam excitation to compensate for shot-to-shot variations in the probe laser intensity. Both the probe and reference beams were passed through a narrow band interference filter (centered at 488 nm) at the same angle of incidence, as shown in the figure, to compensate both beams equivalently for spectral chirping of the dye laser. The timing of the nominally 200 nsec dye laser pulse was adjusted to probe the gas medium approximately 700 nsec after the initiation of e-beam excitation to allow for buildup of gain within the gas. The pulsed dye laser was used with the 0.5 m chamber so that Figure 5-5 includes the 4 pass configuration. The reference detector in these experiments was an ITT F4000 S-1 photodiode operated at 2500 V. The pulsed



8: 04551

Figure 5-5. Experimental Setup for XeF (C → A) Pulsed Gain/Absorption Measurements.

gain measurements were carried out near 488 nm using LD490 (Exiton Chemical Co.) laser dye.

The 1 m laser chamber was used for all oscillator experiments. A stable optical cavity was formed using a 2.17 m radius of curvature output coupler coated for 99 percent reflectivity at 480 nm located 1.3 m from either a 2.17 or a 1.49 m radius of curvature mirror coated for maximum reflectivity at 480 nm. The mirror coatings were designed for greater than 85 percent transmission at 350 nm and were deposited on 1 inch diameter, BK-7 substrates. In addition, the second surfaces of the substrates were AR coated at 350 nm. All cavity mirrors were fabricated by the Perkin-Elmer Corporation, and internal cavity optics were used throughout. Mirror alignment was accomplished external to the chamber using a three point adjustment mount connected to the laser chamber by a metal bellows assembly.

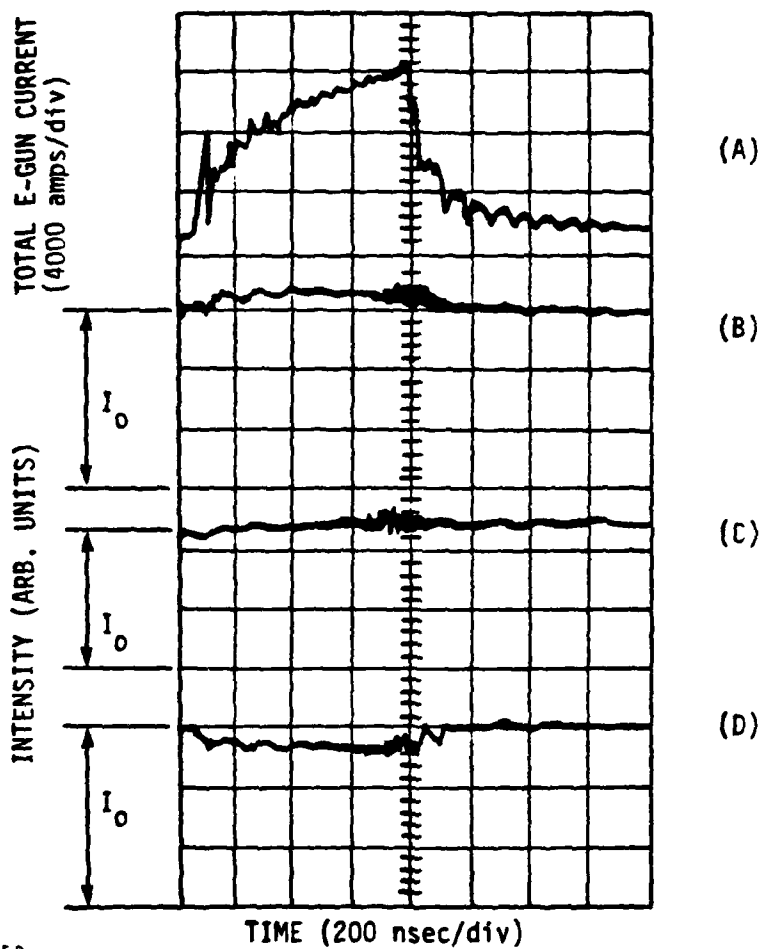
Time integrated fluorescence and laser spectra were measured using a 0.5 m Czerny-Turner spectrometer equipped with a 600 groove/mm grating blazed at 500 nm with an approximate f/8 aperture. The spectrometer was aligned along the optical axis of the photolytic chamber, and radiation from the e-beam excited medium was focused onto the slit to effectively fill the spectrometer aperture. Spectra were recorded on Kodak Royal Pan film at approximately 0.14 nm resolution. Emission intensities were more than sufficient to permit single pulse exposures. Spectra were analyzed from densitometer traces of the exposed film and were corrected for variations in film sensitivity between 440 and 540 nm. Spectra were calibrated using Hg and Xe emission lines produced by conventional penray lamp

sources.

Experimental Results

Gain measurements were carried out using gas mixtures composed of 0.25 percent Xe and 0.12 percent of either NF_3 or F_2 dilute in either Ne or Ar. Total pressures of Ne mixtures were varied between 2 and 5 atm; Ar mixture pressures were typically 1 to 2 atm. When the cw laser probe was tuned to 488.0 nm, Ne mixtures exhibited net gains of approximately 5×10^{-4} and $2 \times 10^{-4} \text{ cm}^{-1}$ with NF_3 and F_2 , respectively, as the F donors. The gain nearly doubled when the mixture containing F_2 was cooled to -20°C .

Figure 5-5 - 5-6 shows representative oscillographic data obtained with the cw laser probe for Ne mixtures using the two pass optical configuration. The e-gun current profile is included for comparison of the time evolutions of the probe signal with that of the e-beam excitation pulse. The maximum gain measured was observed with 5 atm of the Ne mixture, as shown in (B). As can be seen in the figure, the small magnitude of the net gain obtained using the two pass configuration results in a relatively large uncertainty for the measurement. Nevertheless, the increase in signal shown in (B) was reproducible, and the calculated gain of $5 \times 10^{-4} \text{ cm}^{-1}$ is reliable to within a factor of two. When the pressure of the Ne mixture was decreased to 2 atm, the net gain decreased to approximately zero, as shown in (C). When the probe laser was tuned to 514.5 nm, Ne mixtures exhibited absorption, as illustrated in (D).



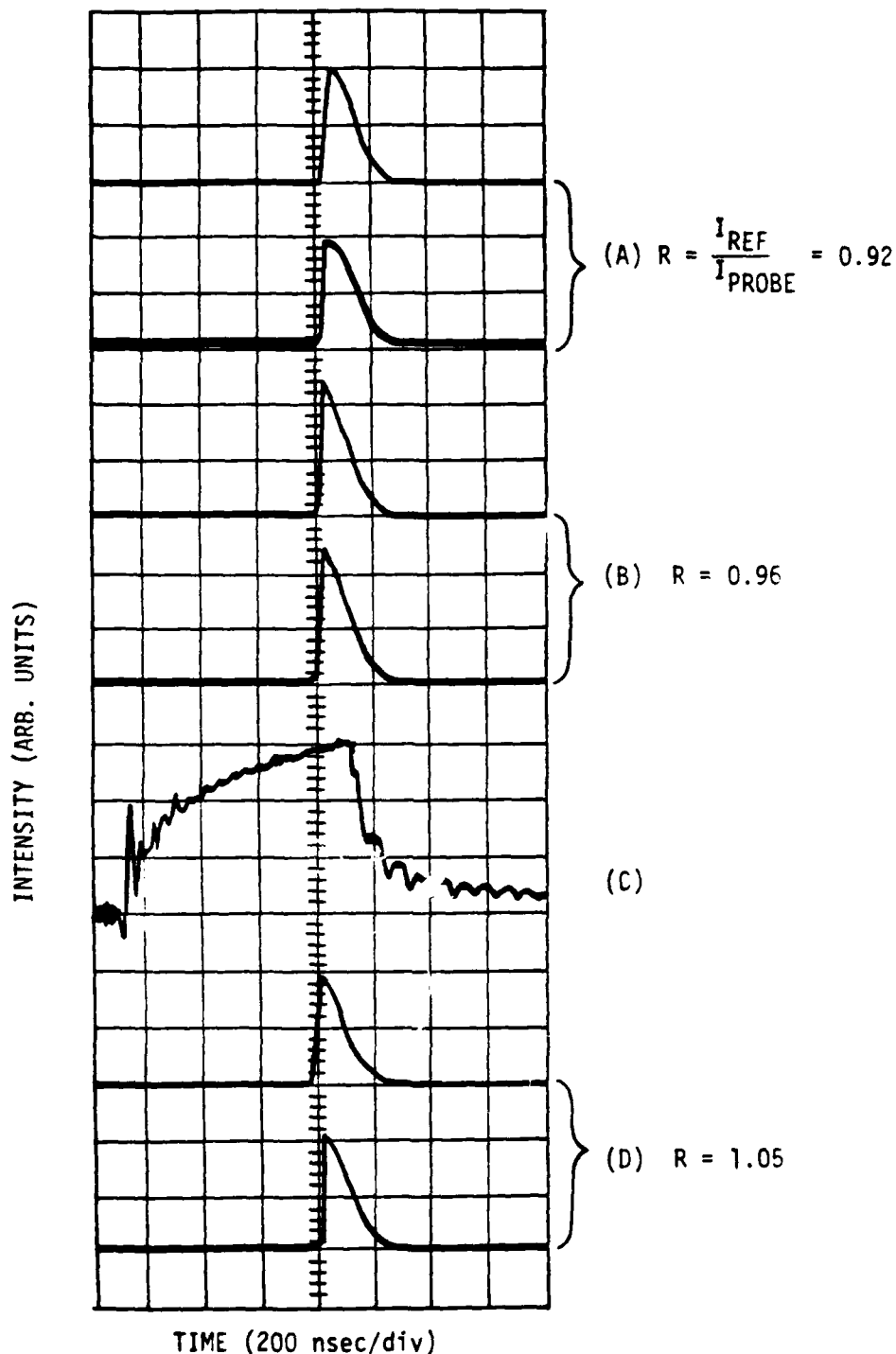
81 04552

Figure 5-6. Room Temperature Gain/Absorption Data Obtained Using the cw Ar^+ Laser Probe. Mixture composition: 0.25% Xe/0.12% NF_3 in Ne. (A) E-gun current Profile, (B) 5 atm mixture, 488.0 nm probe, (C) 2 atm mixture, 488.0 nm probe, (D) 5 atm mixture, 514.5 nm probe. Initial probe laser intensities are indicated to the left of (B), (C), and (D).

Gain measurements were restricted to 488.0 nm in Ar mixtures since intense absorption at 514.5 nm has been observed previously in e-beam excited Ar. A net gain of approximately $5 \times 10^{-4} \text{ cm}^{-1}$ was measured for the Ar mixtures with F_2 , but net absorption was measured when NF_3 was the F donor or when the F_2 containing mixture was cooled to $-24 \text{ }^\circ\text{C}$.

The net gains measured using the pulsed dye laser probe were in agreement with cw probe laser data for both Ne and Ar mixtures to within the accuracy of the measurements. Data obtained for 1 atm of a 0.12% F_2 + 0.25% Xe + Argon mixture using the pulsed probe are shown in Figure 5-7. The ratio of reference to probe beam intensity before and after e-beam excitation varied between 0.92 and 0.96 despite efforts to compensate for output intensity fluctuations and spectral chirping. However, the intensity ratio during e-beam excitation (at the approximate 750 nsec probing time) lies outside the limits of uncertainty defined by the fluctuations of the ratio in the absence of excitation. The resultant net gain was calculated to be $-5 \times 10^{-4} \text{ cm}^{-1}$. Since the spectral bandwidth of the grating tuned dye laser (of the order of 10 cm^{-1}) was much broader than that of the cw laser probe, the agreement of pulsed and cw probe data indicates that absorption of the cw probe beam by argon ions within the e-beam excited medium does not influence the measured net gain in Ar mixtures.

The results of the gain experiments are summarized in Table 5-1. The data indicated that 0.25% Xe/0.12% NF_3 in Ne and 0.25% Xe/0.12% F_2 in Ar were the most promising mixtures to try in room temperature oscillator experiments. In addition, Xe/ F_2



81 04553

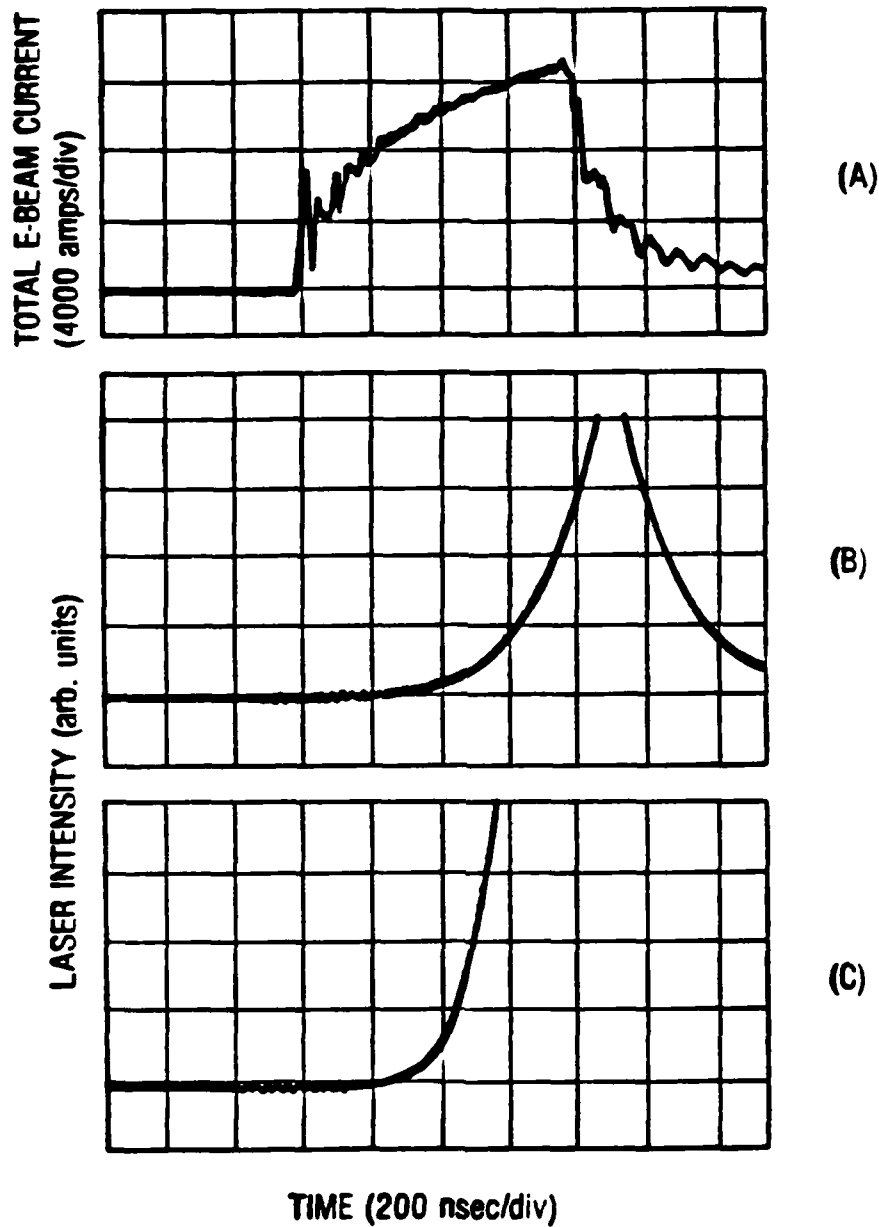
Figure 5-7. Room Temperature Gain Data Obtained at 488.0 nm With the Pulsed Dye Laser Probe. Mixture composition: 1 atm 0.25% Xe/0.12% F₂ in Argon. Top trace of (A), (B), and (D) is the reference signal; bottom trace of (A), (B), and (D) is the probe signal. (A) Before e-beam pulse, (B) after e-beam pulse, (C) e-gun current profile, and (D) during e-beam pulse. (A), (B), and (D) are on the same scale. Net gain $\sim 5 \times 10^{-4} \text{ cm}^{-1}$ (2-m total path length).

Table 5-1. Summary of XeF (C → A) Gain/Absorption Data

% Xe	%NF ₃	%F ₂	Diluent	P(atm)	λ (nm)	Net gain (cm ⁻¹)	Net Abs (cm ⁻¹)	Probe Laser	Temp. (°K)
.24	.12	-	Ne	4-5	488	5 x 10 ⁻⁴		CW Ar ⁺	295
.5	.12	-	Ne	5	514.5	< 5 x 10 ⁻⁴	5 x 10 ⁻⁴	CW Ar ⁺	295
.24	-	.12	Ne	4	488	< 5 x 10 ⁻⁴	5 x 10 ⁻⁴	Pulsed Dye	295
.24	-	.12	Ar	1-2	488	~ 3 x 10 ⁻⁴		CW Ar ⁺	295
						~ 5.8 x 10 ⁻⁴		CW Ar ⁺	253
						5 x 10 ⁻⁴		Pulsed Dye	295
.24	.12	-	Ar	1	488	~ 5 x 10 ⁻⁴	< 5 x 10 ⁻⁴	CW Ar ⁺	295
							5 x 10 ⁻⁴	CW Ar ⁺	249
								Pulsed Dye	295

mixtures dilute in Kr were also used in laser experiments since the rate for mixing of the B and C states by Kr exceeds the rate by Ar by a factor of 4, and the quenching rate of the C state by Kr is no faster than the rate by Ar at equivalent e-beam stopping powers. In addition, information from the kinetic modeling studies indicated that Kr might effectively lower the concentrations of excited xenon species (e.g., Xe^{**}), tentatively identified as absorbers in Ne and Ar mixtures, without appreciably increasing absorption via Kr related species (e.g., Kr_2^+).

The Ne/Xe/NF₃ mixture failed to reach threshold for pressures between 3 and 5 atm and e-beam pulse durations of up to 950 nsec. The Ar and Kr based mixtures achieved oscillation, and time resolved laser profiles obtained under conditions of equivalent stopping powers are shown in Figure 5-8. With Ar diluent the laser operated close to threshold, and the peak intracavity flux was ~ 4 kW/cm², considerably below the estimated 1 mW/cm² saturation flux. The gain calculated from the ringup time in Figure 5-8b is approximately 2×10^{-4} , in reasonable agreement with the net gain measured at 488.0 nm in the absence of cavity losses for the Ar mixture. The increase in emission intensity subsequent to e-beam termination and the relatively slow emission decay rate are consistent with the high Q cavity used in these experiments. The rate of increase in laser intensity was also observed to increase slightly following e-beam termination indicating that losses in the gas medium are greater during e-beam excitation. This observation is illustrated in Figure 5-9 for the case of 2 atm of 0.12% F₂/0.25% Xe in Ar. However, when the average e-



81 04554

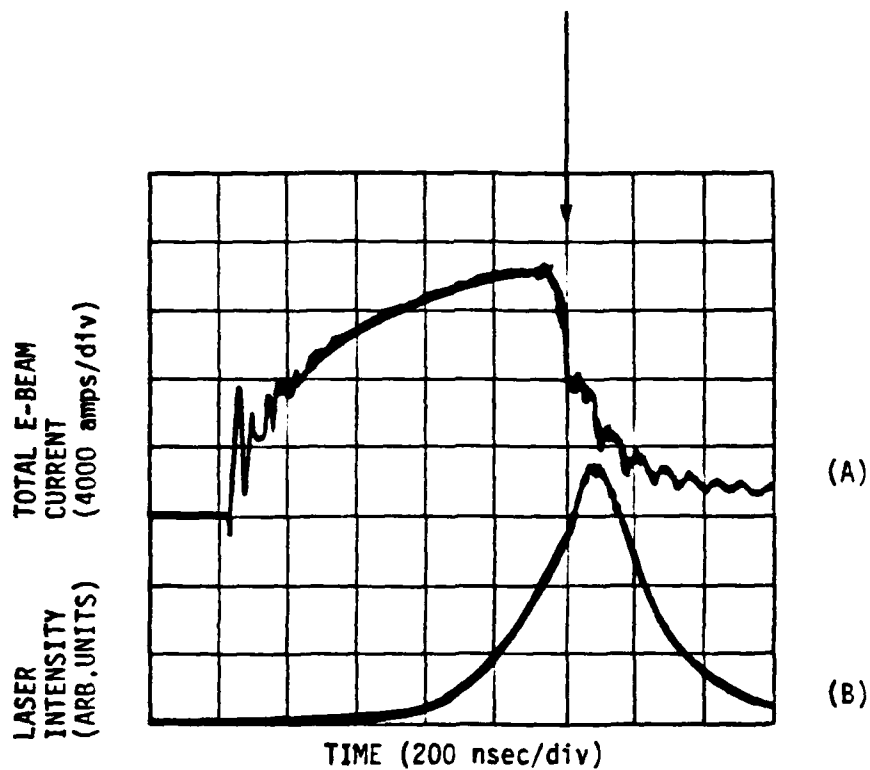
Figure 5-8. Time Resolved Profiles of (A) the Total E-beam Current, (B) Laser Emission From 2 atm of 0.25 Percent Xe + 0.12 Percent F₂ in Ar, and (C) Laser Emission From 1 atm of 0.5 Percent Xe + 0.25 Percent F₂ in Kr. The sensitivity of (B) is twice that of (C).

beam current density over the excitation volume was decreased by a factor of two, the laser turn on time effectively doubled, as shown in Figure 5-10 where experimental conditions were unchanged from Figure 5-9 except for an increase in the e-gun anode-cathode spacing from 5.5 to 7 cm. Despite the somewhat shorter duration of the e-beam pulse in Figure 5-10, the laser has nevertheless begun to turn on by the time of e-beam termination at 800 nsec. In Figure 5-9, where $j_{eb}(\max)$ is roughly 1.7 times that in Figure 5-10, the laser turn on time is at approximately 400 nsec after the start of the excitation pulse.

Substitution of Kr and Ar considerably improved the performance of the laser. The gain for the Kr mixture was estimated from the ring up time in Figure 5-8c to be $\sim 4 \times 10^{-4} \text{ cm}^{-1}$. Results of other experiments for the same excitation conditions as used in Figure 5-8 (but with the laser trace fully on scale) indicated that the peak intracavity flux increased a factor of 20 substituting Kr for Ar. The maximum laser intensity thus far measured occurred for the second shot on the Kr mixture with a 950 nsec e-beam pulse and corresponded to a peak intracavity flux of $\sim 1.3 \times 10^5 \text{ W/cm}^2$. The corresponding laser output energy was of the order of 1 mJ based on the calibrated photodiode sensitivity, the approximate transmission of the filters and attenuators used, and the diameter and transmission of the output coupler.

In order to determine whether the improved laser performance could be ascribed to an increase in small signal gain the fluorescence was monitored for both Ar and Kr based mixtures under conditions of equivalent e-beam stopping powers. In these experiments the laser

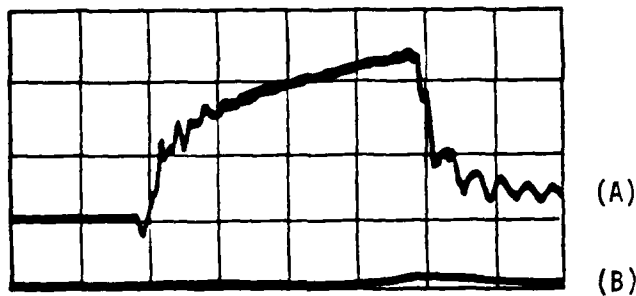
E-BEAM TERMINATION



81 04555

Figure 5-9. Time Resolved Profiles of (A) the Total E-beam Current and (B) Laser Emission from 2 atm of 0.25% Xe + 0.12% F₂ in Ar. The e-gun anode-cathode spacing was 5.5 cm.

LASER INTENSITY TOTAL E-BEAM CURRENT
(ARB UNITS) (4000 amps/div)



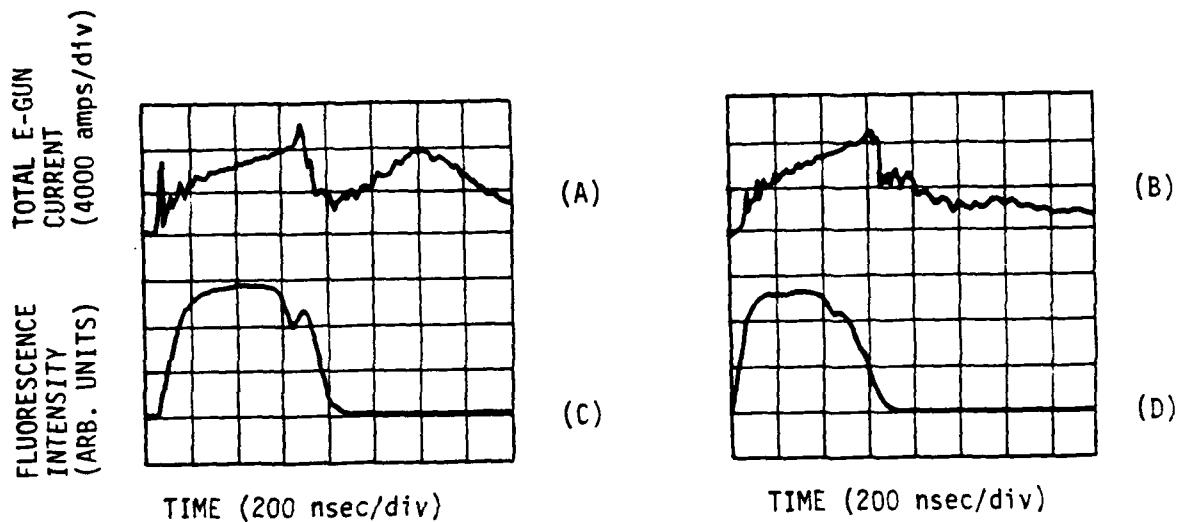
01 04556

Figure 5-10. Time Resolved Profiles of (A) The Total E-beam Current and (B) Laser Emission From 2 atm of 0.25% Xe + 0.12% F₂ in Ar. The e-gun anode-cathode spacing was 7 cm. Sensitivity of (B) equals that of Figure 5-9(B).

cavity mirrors were removed, and the F4000 S-5 photodiode was positioned to monitor fluorescence approximately along the longitudinal direction of the photolytic chamber. The fluorescence was attenuated by about two orders of magnitude and passed through an interference filter centered at 490 nm with an approximate 100 nm (FWHM) bandwidth.

Results of these experiments are summarized in Figure 5-11. The magnitude of the fluorescence intensity was essentially unchanged substituting Kr for Ar, indicating that the observed improvement in laser performance with Kr diluent is consistent with a decrease in broadband absorption rather than an increase in small signal gain over the laser bandwidth.

Time integrated fluorescence and laser spectra are shown in Figure 5-12 for both Ar and Kr mixtures. Fluorescence emission extended for \sim 540 nm to below 420 nm with maximum intensity near 460 nm. Laser emission occurred principally between 470 and 500 nm with maximum intensity near 495 nm. The broad emission features near 500 nm in the fluorescence (see Figure 5-12) correspond to KrF emission in the second order of the spectrometer. Absorption features are both more numerous and intense in the Ar mixture spectra than in the Kr mixture spectra. Absorption features in the fluorescence spectra have been identified with Xe(I) and Kr(I) transitions, as shown in Figure 5-12. Specifically, the lines have been assigned in every case to transitions which terminate on the 1S (Paschen notation) states of Xe and Kr. Kr was evidently present as an impurity in the Ar mixtures. Additional unidentified absorption lines appear in the laser



B1 04557

Figure 5-11. Time Resolved Profiles of (A) and (B) the Total E-gun Current, (C) Fluorescence from 2 atm 0.25% Xe/0.12% F_2 in Ar, and (D) Fluorescence from 1 atm 0.5% Xe/0.25% F_2 in Kr. (C) and (D) Are On the Same Scale.

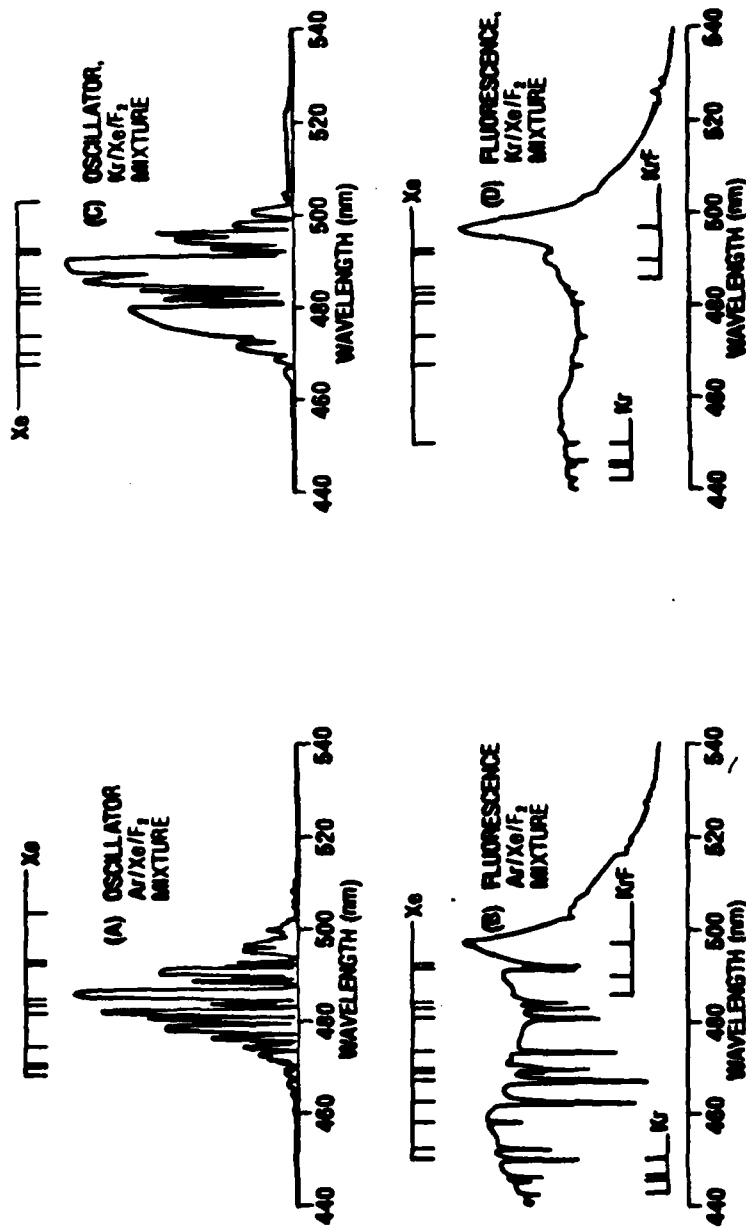


Figure 5-12. Time Integrated Spectra From (A) the XeF C-A Oscillator and (B) Fluorescence, Using 0.25 Percent Xe/0.12 Percent F₂ in Ar, (C) the XeF C-A Oscillator and (D) Fluorescence Using 0.25 Percent Xe/0.12 Percent F₂ in Kr. Spectral intensities are normalized to the same (arbitrary) scale. Spectra were obtained from densitometer traces (see text) Absorption lines assigned to atomic transitions in Xe and Kr are indicated along with KrF emission features observed in the second order of the spectrometer.

81 04558

spectra.

It is clear from the time resolved emission data that for the e-beam excitation conditions used, the performance of the XeF C-A laser is limited by cavity flux buildup. Spectral data confirm the potential broadband tunability of an e-beam pumped system, although laser performance may be limited by broadband absorption during e-beam excitation. Substitution of Kr for Ar diluent dramatically improved laser performance and increased the intracavity laser intensity to within a factor of 10 of the estimated saturation flux for the system.

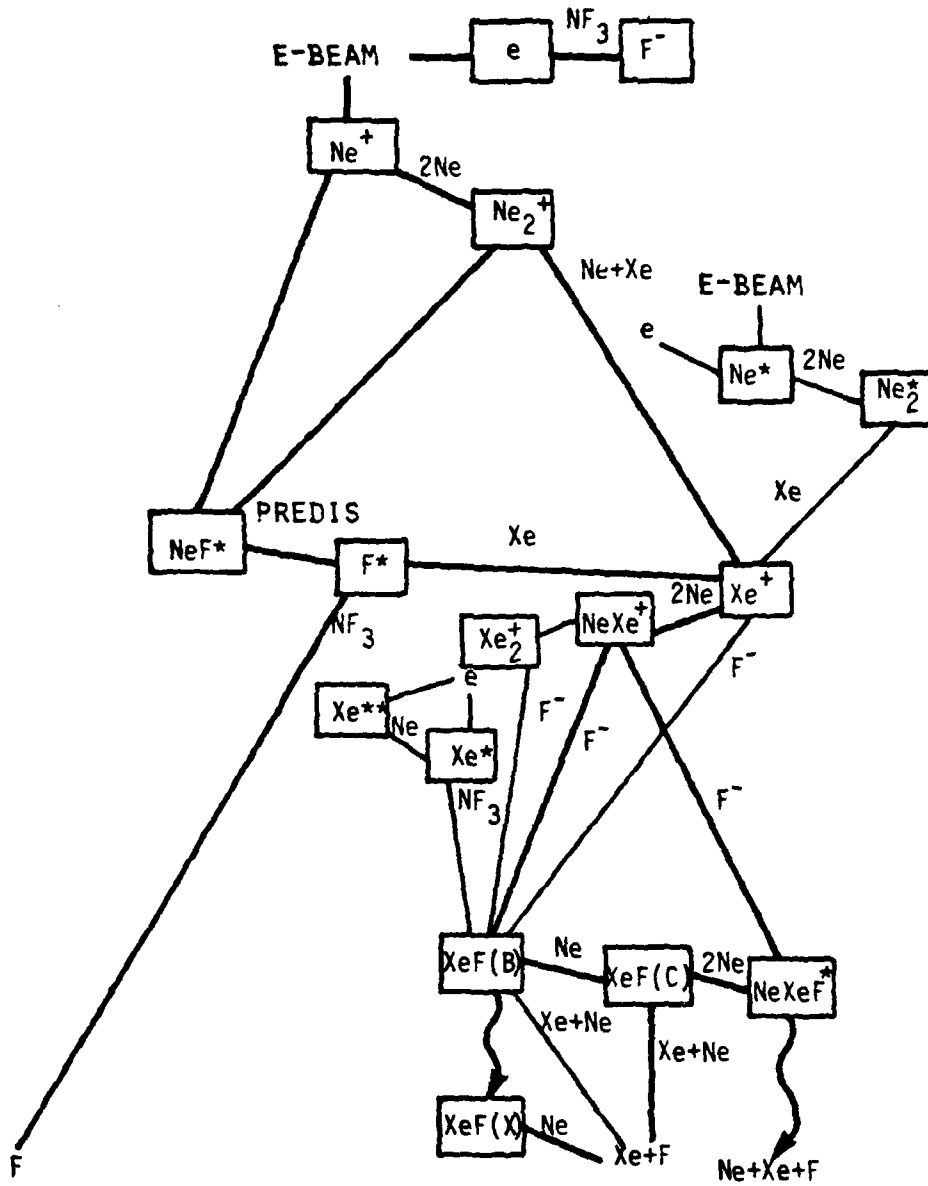
Modeling Section

The development of a kinetic model for the XeF system was undertaken in this program both to facilitate the interpretation of experimental results and to provide predictive capability for future system designs. The detailed formulation of the model incorporates both light and heavy particle kinetic processes to determine numerically the time varying concentrations of species which are believed to influence the performance of the XeF (C-A) laser system using electron beam excitation. The dominant formation kinetics depend on the rare gas diluent, the halogen donor, and the total operating pressure, although the ultimate choice of the optimum gas mixture for the laser depends not only on the formation kinetics but also on intrinsic absorption of XeF B and C state radiation by halogen species (e.g., F^- , F_2) and rare gas dimer ions and neutral species such as Ar_2^+ , Ne_2^+ , Kr_2^+ , Xe_2^+ , Ne_2^* , and Xe^{**} (where $**$ denotes excitation to states higher lying than 6s).

The specific intent of the modeling program was to investigate electron beam excited mixtures of Xe and either NF_3 or F_2 , dilute in either Ne, Ar, or Kr, as a function of both gas composition and temperature in order to determine conditions which maximize the gain on the 460 nm C-A transition. The approach to the modeling was to modify an existing XeF (B-X) code written for Ne diluent to allow for either Ar or Kr diluents as well as to include C state kinetics.

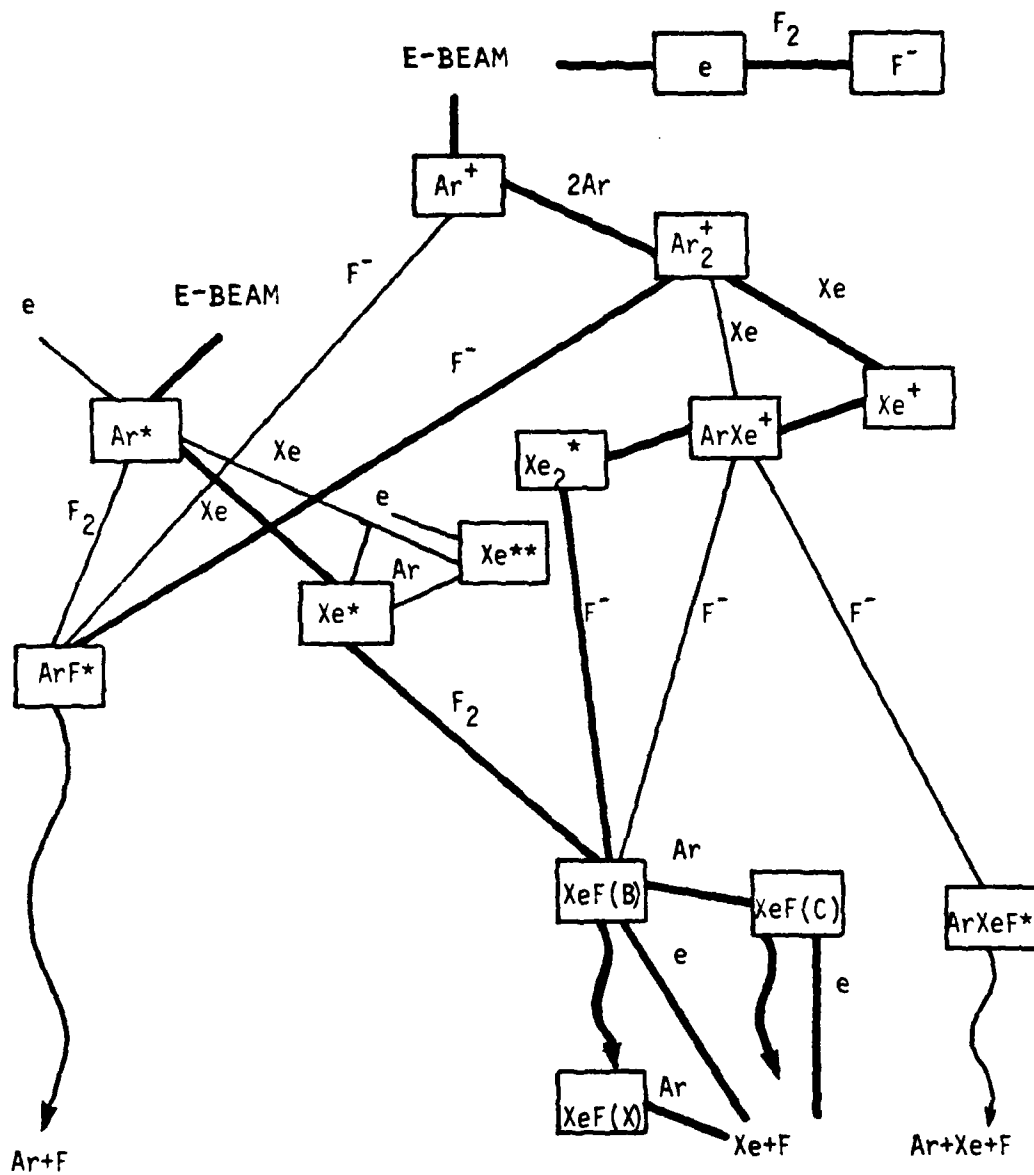
Experimental operating pressures were chosen so that the optical axis of the system was located close to the region of maximum e-beam energy deposition predicted by electron scattering codes. The assumption was made that the electron velocity distribution was Maxwellian and that energy deposition was uniform throughout the excitation volume. The assumption of a Maxwellian distribution was justified by the high pressure (1-5 atm) and e-beam current densities ($< 10 \text{ A/cm}^2$) used in the experiments. E-beam uniformity measurements carried out prior to the start of this work established that energy deposition over the length of the excitation region was uniform to within $\pm 10\%$. Results from these experiments were then used in the kinetic model to calculate the average e-beam power deposition for the XeF experiments.

The principal formation pathways which have been included in the modeling of the XeF system are shown schematically in Figures 5-13, 5-14, and 5-15 for the cases of Ne, Ar, and Kr diluents, respectively. In these diagrams, energy increases in the vertical direction. Pathways which are most influential in the formation of XeF (B or C state) are indicated by heavy lines; less influential pathways are indicated by light



80 03699

Figure 5-13. XeF Formation Pathways: Ne Diluent.



6C 0369E

Figure 5-14. XeF Formation Pathways: Ar Diluent.

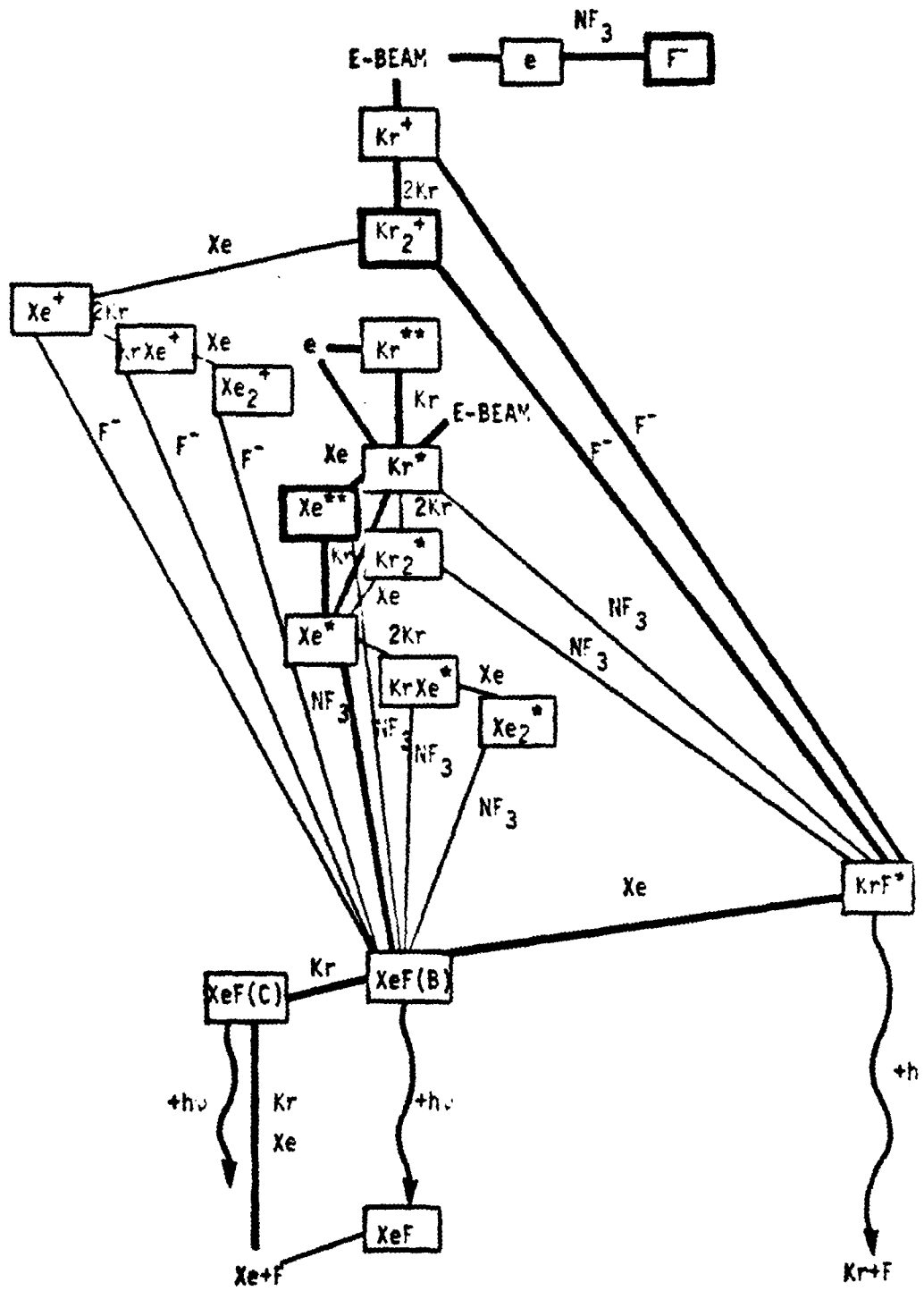


Figure 5-15. XeF Formation Pathways: Kr Diluent.

lines. Wavy lines depict the emission of a photon. Species which are either known or have been invoked to absorb either B or C state radiation have been heavily outlined. The label 'e-beam' denotes an energy deposition source term for primary electrons. The label 'e' denotes secondary electrons.

As can be seen in the diagram, once X^+ (X = rare gas diluent) is formed by initial e-beam ionization, significant differences emerge between the principal formation pathways using the different rare-gas diluents. In the cases of Ar and Kr, the singly ionized species are rapidly converted to dimer ions via 3-body collisions. The dimer ions recombine with F^- formed by the dissociative attachment of secondary electrons to the F donor (NF_3 or F_2). The product of ion-ion recombination is then either ArF^* or KrF^* . In the case of Ne, this same sequence occurs, although direct formation of NeF^* via Ne^+ combining with F^- is also important. Some of the higher energy rare gas fluorides contribute to the formation of XeF , either directly via the neutral channel by displacement or indirectly via the ionic channel.

In the case of Ne diluent, formation of $XeF(B)$ occurs primarily via ionic channels. With Ar diluent, the excitation energy is partitioned between neutral channels (via Ar^* and Xe^*) and ionic channels (via Xe_2^+). With Kr, $XeF(B)$ is formed principally via neutral channels (either directly from KrF^* or indirectly from Kr^{**} and Kr^* via Xe^*). $XeF(B)$ is lost primarily by collisional transfer to the C state and by radiative transfer to $XeF(X)$, although quenching $XeF(B)$ by secondary electrons appears to be important in Ar diluent mixtures. The C state is lost primarily

through collisional quenching (with Ne and Kr diluents) or electron quenching (in Ar mixtures) as well as radiation to the A state.

The incorporation of Kr diluent in the kinetic model results in XeF formation pathways significantly different from those predicted for Ne and Ar. Metastable Kr (Kr^*) lies energetically below Xe^+ so that XeF production via the $\text{Xe}^+ + \text{F}^-$ ion channel is not a principal formation path, and, instead energy is channelled via Xe^* and, more importantly KrF^* . The branching from KrF^* to XeF(B) is assumed to be 100 percent. The only data available concern the rate of disappearance of KrF^* by Xe. This may be due not only to XeF(B) production, but also either a simple quenching of KrF^* or the production of KrXeF^* . This is a potentially significant uncertainty, since the gain on the C-A transition is primarily related to XeF(B) production from KrF^* . This is not a problem with Ar and Ne diluents since XeF production occurs principally via the ionic channels and the C-A gain is insensitive to the fate of ArF or NeF . Finally, the role of principal absorbing species is difficult to assess accurately due to incomplete photoionization and photodissociation cross section data. This is particularly troublesome in modeling the XeF C-A system due to the low magnitude of the small signal gain.

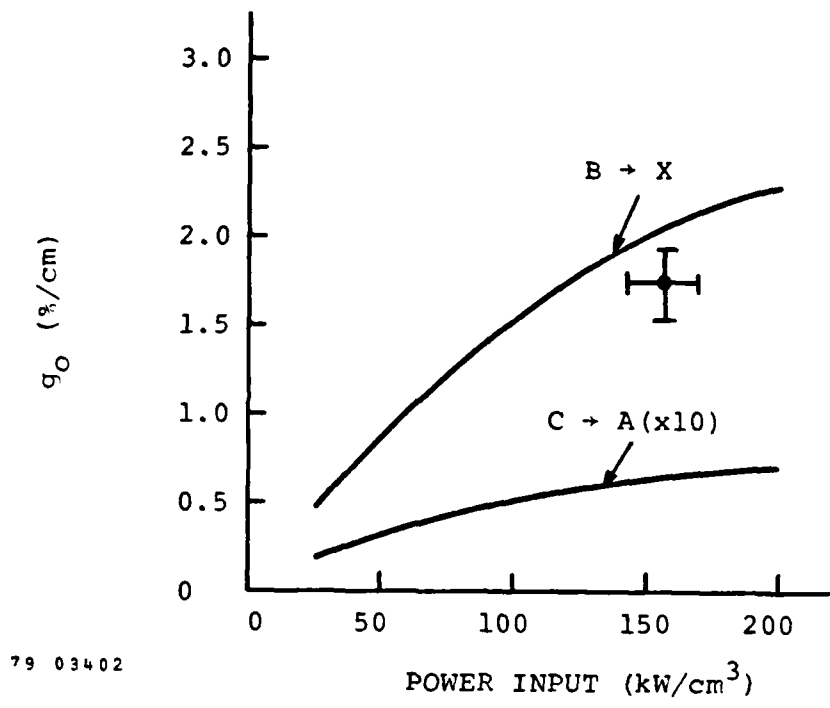
The model predicted lower absorption than that measured by Champagne at NRL even though all the known absorbers and their cross sections had been incorporated into the model. In order to match the absorption measurements, a species Xe^{**} corresponding to higher excited states of Xe^* was introduced. The cross sections used for the photoionization of Xe^{**} by

B and C state radiation, photoionization of Xe_2^* by B state radiation, and photodissociation of Xe_2^* by C state radiation were not known and were treated as adjustable parameters in the modeling calculations.

Results of Code Predictions

Results of code calculations are shown in Figures 5-16 through 5-20. With the exception of Figure 5-17, these figures show calculations of small signal gain, g_0 and the gain to loss ratio, g_0/α , for both the B-X and C-A transitions as a function of power input and for various mixture compositions containing Ne, Ar and Kr diluents. Figure 5-17 shows results of power extraction calculations for the B-X transition using a Ne/Xe/NF₃ mixture. Results for Ne diluent are shown in Figures 5-16 and 5-17; Ar diluent calculations are shown in Figure 5-18; Kr diluent calculations are shown in Figures 5-19 and 5-20. In Figures 5-16, 5-17 and 5-18 data obtained by Champagne at NRL for the B-X transition have been included for comparison with the code predictions. In these instances, the mixture composition, total pressure, and other experimental parameters (where appropriate) have been adjusted to match the NRL experimental conditions as closely as possible. As can be seen, there is good agreement between the experimental results and the code calculations.

Table 5-2 summarizes the code predictions at a 100 kW/cm³ pump power density, taken as representative of experimental excitation conditions typically used. For the Ne/Xe/NF₃ mixture both g_0 and g_0/α are lower for the C-A transition than for the B-X. Laser performance on the B-X transition is predicted to be



_____ MSNW CODE
 ┌───┴───┐ NRL (B → X) EXPERIMENT

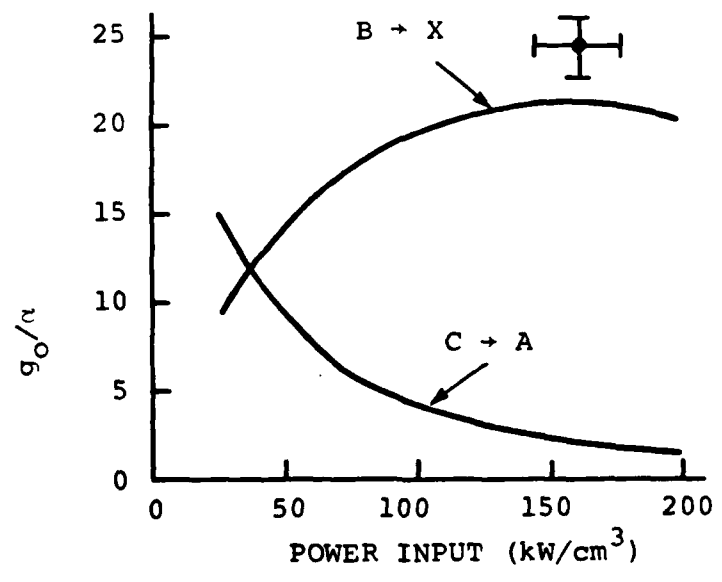
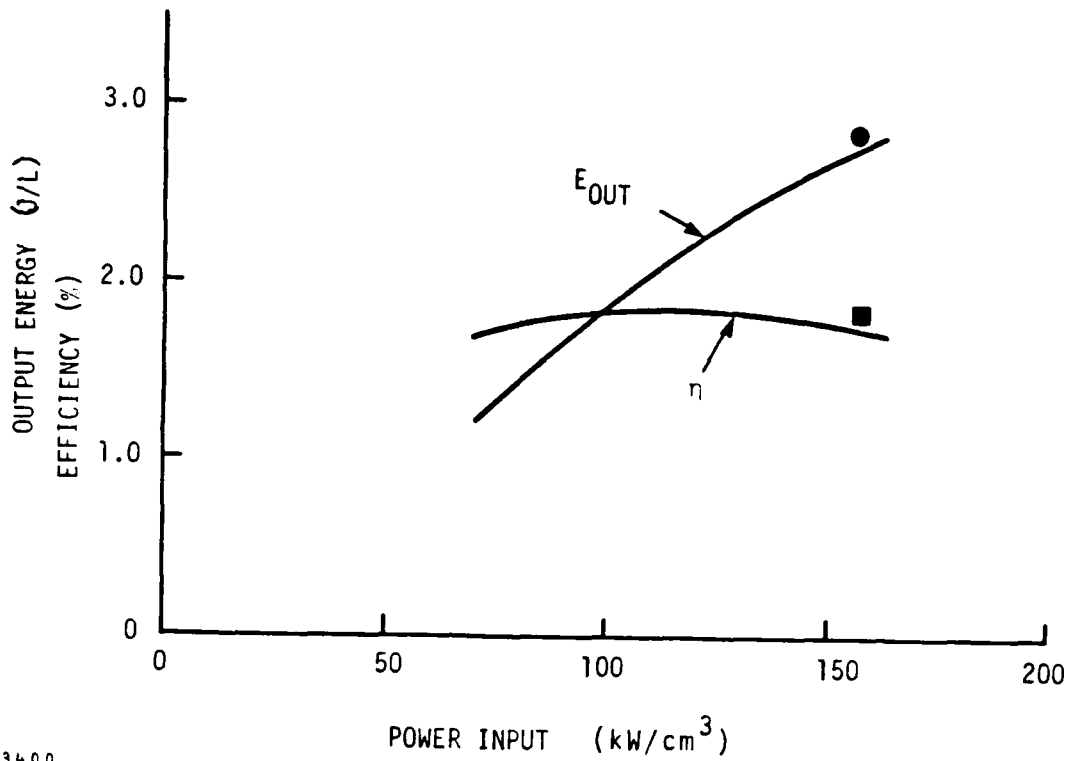


Figure 5-16. Code Predictions for Ne/Xe/NF₃ Mixtures.



Ne/Xe/NF₃ = 99/0.18/0.06
 P = 5 atm
 T₀ = 300 °K
 τ_{eb} = 1 μsec
 L_{cav} = 100 cm
 T_m = 50%

— MSNW CODE
 ● E_{OUT}
 ■ η } CHAMPAGNE EXPERIMENT

Figure 5-17. XeF* (B→X) Power Extraction for Ne/Xe/NF₃ Mixtures.

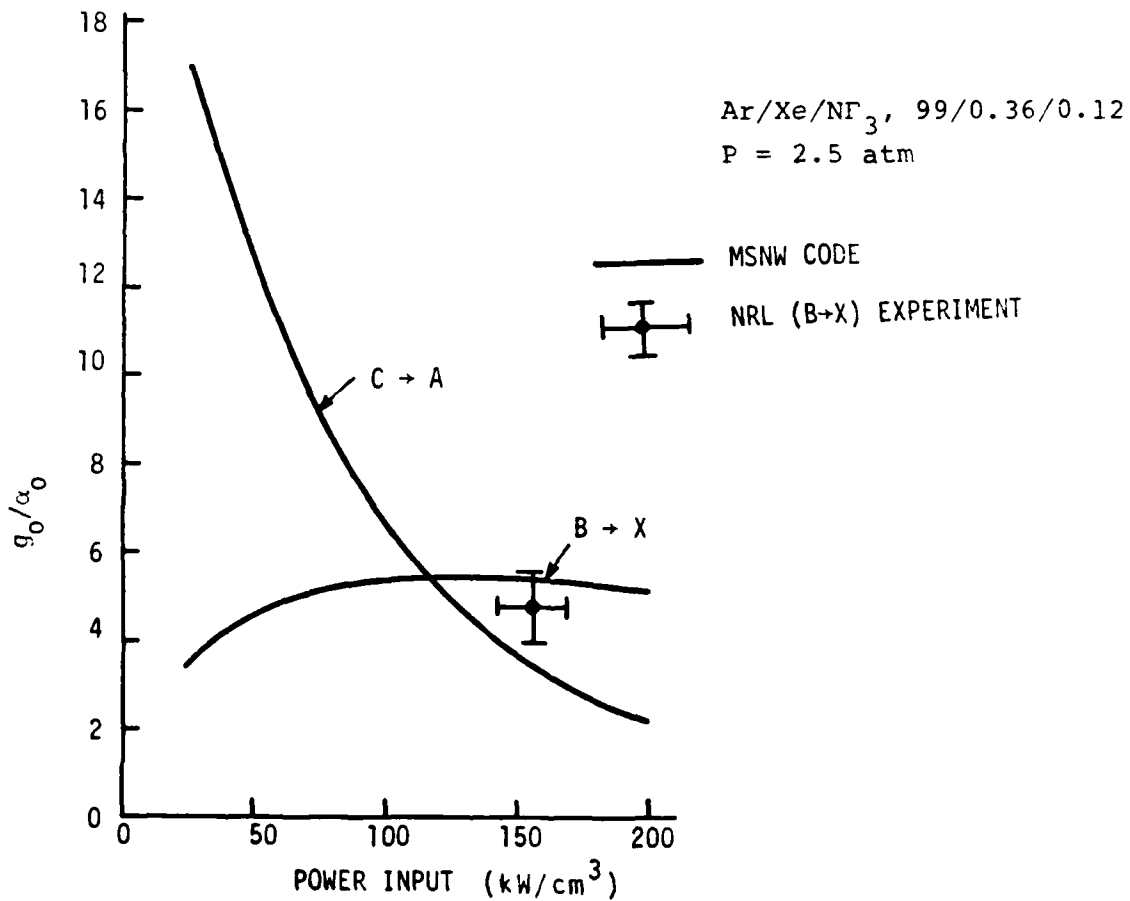
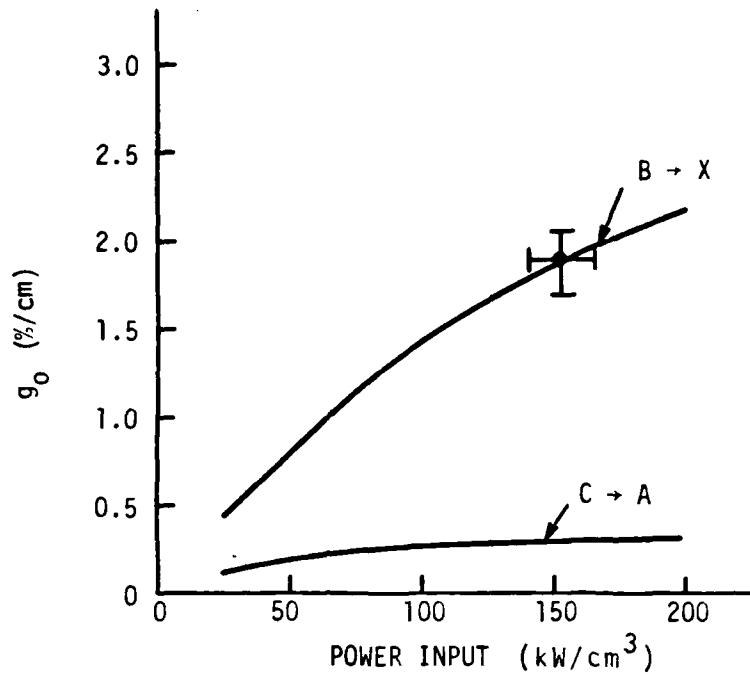


Figure 5-18. Code Predictions for Ar/Xe/NF₃ Mixtures.

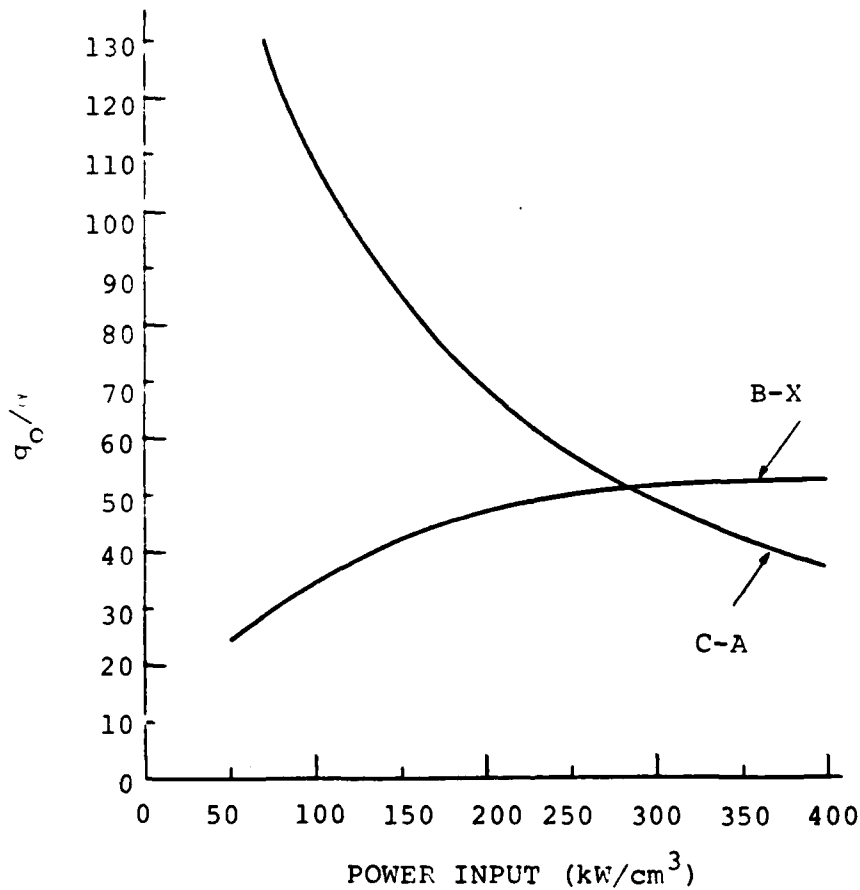
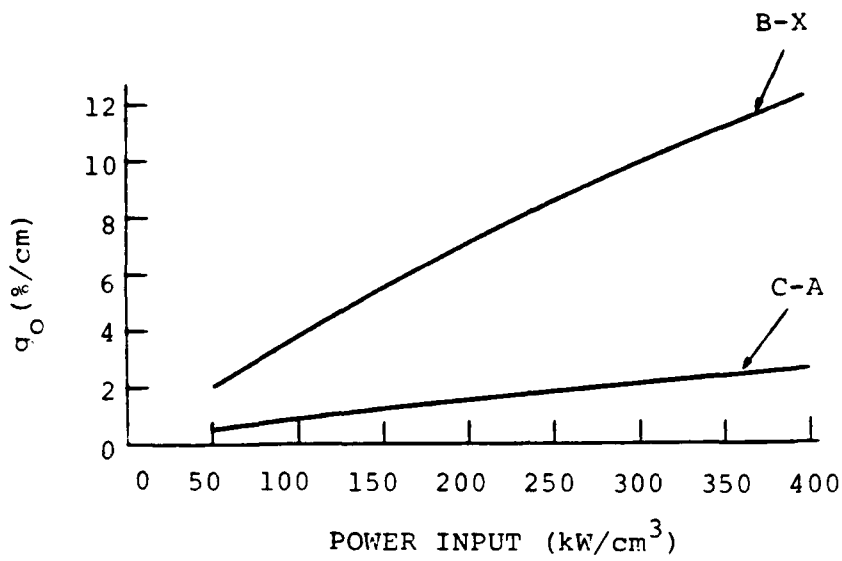


Figure 5-19. Code Predictions for XeF Performance Kr Diluent: Kr/Xe/NF₃ (98/1/1), P = 1.1 atm.

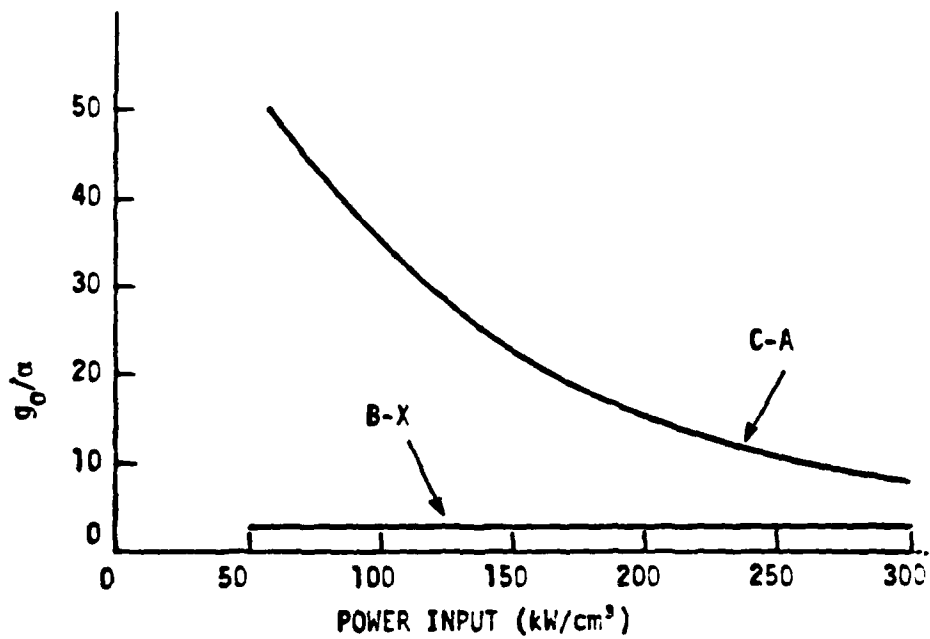
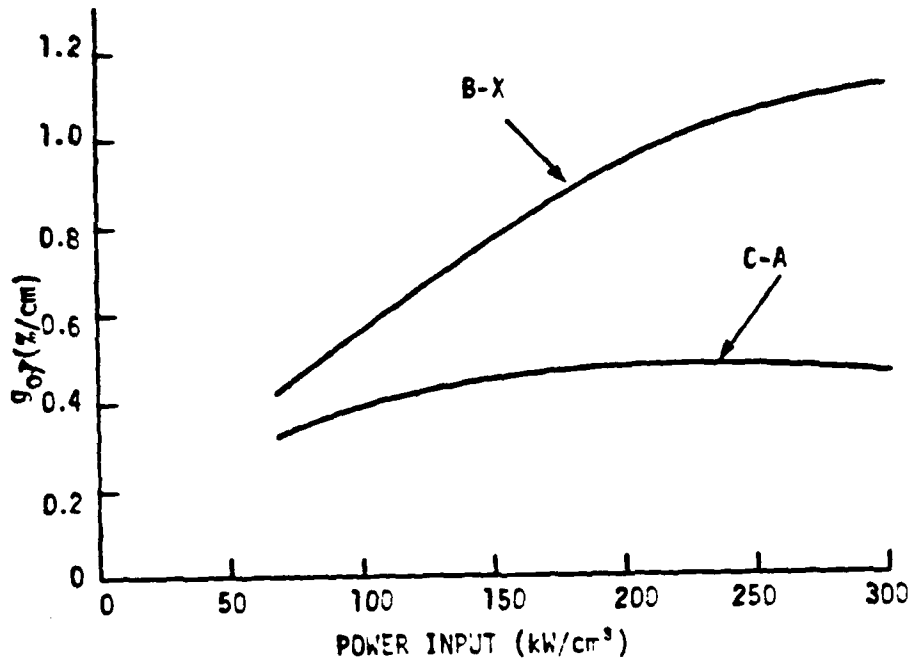


Figure 5-20. Code Predictions for XeF Performance: Kr/Xe/F₂ (99/0.5/0.25), P = 1 atm.

Table 5-2

Summary of Code Predictions at 100 kW/cm³ Pump Power Density

Mixture Composition	P (atm)	$g_0(B \rightarrow X)$		$g_0(C \rightarrow A)$		$g_0^{-\alpha}(B \rightarrow X)$		$g_0^{-\alpha}(C \rightarrow A)$	
		(%/cm)	(%/cm)	(%/cm)	(%/cm)	(%/cm)	(%/cm)	(%/cm)	(%/cm)
Ne/Xe/NF ₃ (99.76/.18/.06)	5	1.5	20	0.05	4	1.4	0.04		
Ar/Xe/NF ₃ (99.52/.36/.12)	2.5	1.5	5.5	0.25	6.5	1.2	0.21		
Kr/Xe/F ₂ (99.25/.5/.25)	1	0.55	2.5	0.4	35	0.33	0.39		
Kr/Xe/NF ₃ (.9/1/1)	1.1	3.8	35	0.8	110	3.7	0.79		

somewhat worse substituting Ar for Ne at equivalent stopping powers due to increased absorption, and this has been observed experimentally using NF_3 as the F donor. Both g_0 and g_0/α are predicted to increase for the C-A transition using Ar diluent. The use of Kr diluent results in a further increase in g_0 for the C-A transition although the principal effect is a substantial increase in g_0/α . The gain and loss for the B-X transition are clearly very sensitive to the F donor with Kr diluent, and the Kr/Xe/ F_2 mixture is predicted to optimize performance on the C-A transition relative to the B-X transition.

For purposes of comparison with measured net gain data the kinetic code was run for 4 atm of a Ne/Xe/ NF_3 (99/0.25/0.12) mixture and 2 atm of an Ar/Xe/ F_2 (99/0.25/0.12) mixture. The results (not shown in Table 5-2) predict net gains of 0.09 percent/cm and 0.189 percent/cm for the Ne and Ar based mixtures, respectively, at 100 kW/cm^3 for the C-A transition. Although these results differ from the net gains predicted for the Ne and Ar mixtures included in Table 5-2, the trend shown in the table when changing from Ne to Ar to Kr is preserved.

The measured net gains for the Ne and Ar mixtures were both ~ 0.05 percent/cm so that the code predictions are too large by at least a factor of two. Due to the uncertainty in the measured gains (discussed in the Experimental Section) it is not clear that the factor of two difference in the predicted gains between the Ne and Ar mixtures is significant. However, the difference between the predicted gains for the Ar/Xe/ F_2 and Kr/Xe/ F_2 mixtures is also consistent with calculated gains based on the observed laser cavity

ring up times (see the Experimental Section), although again the magnitudes of the predicted gains are too large. In the case of the Kr/Xe/NF₃ mixture the uncertainty in the predicted gain may be even greater since the B-X transition failed to reach threshold experimentally whereas B-X laser emission was obtained using both 5 atm of the Ne/Xe/NF₃ (99.76/0.18/0.06) mixture and 2 atm of Ar/Xe/F₂ (99.63/0.25/0.12) mixture. The Kr/Xe/NF₃ mixture was not tried on the C-A transition.

In summary, the modeling code presently predicts net gains for the C-A transition which vary for different diluents at least qualitatively in accordance with experimental observations. Code prediction for gain on the B-X transition are in good agreement with previous data reported by Champagne. In all cases for which comparisons can be made with experiments, the magnitudes of the predicted net gains for the C-A transition appear to be too large. The code predictions for the Kr/Xe/NF₃ mixture are in qualitative disagreement with experiment at the present time for the B-X transition and data are not yet available for comparison with the predictions for the C-A transition.

REFERENCES

1. W.K. Bischel, H.H. Nakano, D.J. Eckstrom, R.M. Hill, D.L. Huestis, and D.C. Lorents, Appl. Phys. Lett. 34, 565 (1979).
2. H.T. Powell, "Kinetics and Lasing Measurements in Photolytically Excited XeF," 32nd Annual Gaseous Electronics Conference, Session E, Pittsburgh, PA, October, 1979, unpublished.
3. R. Burnham, Appl. Phys. Lett. 35, 48 (1979).
4. C.H. Fisher, R.E. Center, G.J. Mullaney, and J.P. McDaniel, Appl. Phys. Lett. 35, 26 (1979).
5. C.H. Fisher, R.E. Center, G.J. Mullaney, and J.P. McDaniel, Appl. Phys. Lett. 35, 901 (1979).
6. W.E. Ernst and F.K. Tittel, Appl. Phys. Lett. 35, 36 (1979).
7. R.M. Hill, P.L. Trevor, D.L. Huestis, and D.C. Lorents, Appl. Phys. Lett. 34, 137 (1979).
8. C.H. Fisher, J.P. McDaniel, and R.E. Center, unpublished.
9. The saturation flux was calculated neglecting electron quenching of the C state.

**DATE
FILMED**

1-8